MODELLING OF COMPRESSIVE TESTS ON FRP WRAPPED CONCRETE CYLINDERS THROUGH A NOVEL TRIAXIAL CONCRETE CONSTITUTIVE LAW

Elena FERRETTI and Antonio DI LEO

Bologna Alma Mater (Italy) – Faculty of Engineering – DISTART

ABSTRACT

A novel constitutive law for concrete in monoaxial loading was developed in previous studies[1][2][3]. This law has been extended here to the triaxial field, so as to model composite (FRP) wrapped concrete cylinders. A numerical code is presented, which is able to reproduce experimental results for unwrapped and wrapped cylinders by only setting the number of wrapping sheets. No parameter is introduced to take into account triaxial stress. No calibration is therefore needed. A tool for crack propagation description is proposed, so as to analyse stiffness decreasing during loading. Numerical simulations have been carried out by means of a Cell Method code[4].

Key-words: wrapping, constitutive law, crack propagation, modelling.

INTRODUCTION

In the past fifteen years, strengthening and repair by composite (FRP) flexible sheets had an important diffusion both in U.S.A. and in Japan, in consideration of significant execution and economic advantages. The reinforcement of structural elements through superficial application of FRP sheets is named "wrapping". This technique provides compressed structural elements with a lateral confinement, which is typically a passive confinement.

The effectiveness of passive confinement provided by composite fibrous material generates a notable increase of load capacity and ductility. On the other hand, the beneficial effects of lateral reinforcement on strength and deformation have been recognised since the early days of structural concrete, much before the advent of FRP. If compared to other passive confinement techniques for concrete, like steel spirals and circular or rectangular hoops, the use of FRP sheets looks as an optimal. Actually, to achieve an appreciable design strength improvement with steel spirals, a heavy manufacturing burden is required to realise helicoidally shaped stirrups, very close to each other. Moreover, steel elements are not adequate to strengthen or repair existing buildings, since external application of thin steel sheets implies a burdensome moulding, several problems of installation, and a complicated behaviour under Euler force. On the contrary, FRP sheets have a good fitness to different shapes of cross-section, are easy to lay, and present no problems of instability. Since concrete cover spalls before failure is reached, little increase in strength occurs with steel spirals. FRP sheets would require no cover. Therefore, the loss of strength due to spalling would not occur. Concrete failure theory suggests that confinement reinforcement can be significantly more efficient in resisting compressive force than longitudinal reinforcement. Therefore, the relatively expensive composite material can be used most efficiently as confinement reinforcement. FRP sheets also make it possible to easily improve strength and ductility of any existing structural element without any appreciating increase of mass, due to a high strength-to-weight ratio. This last point makes the use of FRP sheets very convenient in seismic zones. Moreover, wrapping dramatically increases the toughness of concrete columns, and provides an excellent resistance to harsh environmental conditions[5]. Due to the chemical attack and corrosion resistance of composite materials, FRP sheets could provide an excellent alternative to steel reinforcements for externally bonded repair or patch repair. Finally, wrapped structural elements possess a long fatigue life.

It must be noticed that FRPs have vulnerability to fire, UV radiations, and, in certain cases, moisture. Anyway, a coating protection through adequate paints is sufficient to ensure an acceptable durability, minimising maintenance costs.

Experimental results on wrapped concrete cylinders under compression are well known. In Fig. 1, they are qualitatively compared to results on unreinforced and steel reinforced cylindrical specimens, in terms of nominal stress versus average strain curves. From Fig. 1, it can be observed that: -

- The slope of the first ascending branch is more or less identical for all three cases;
- Unreinforced and steel stirrups reinforced specimens exhibit strain-softening behaviour;
- Wrapped specimens does not exhibit strain-softening behaviour;
- The ultimate strain is much higher in wrapped than in unreinforced specimens.

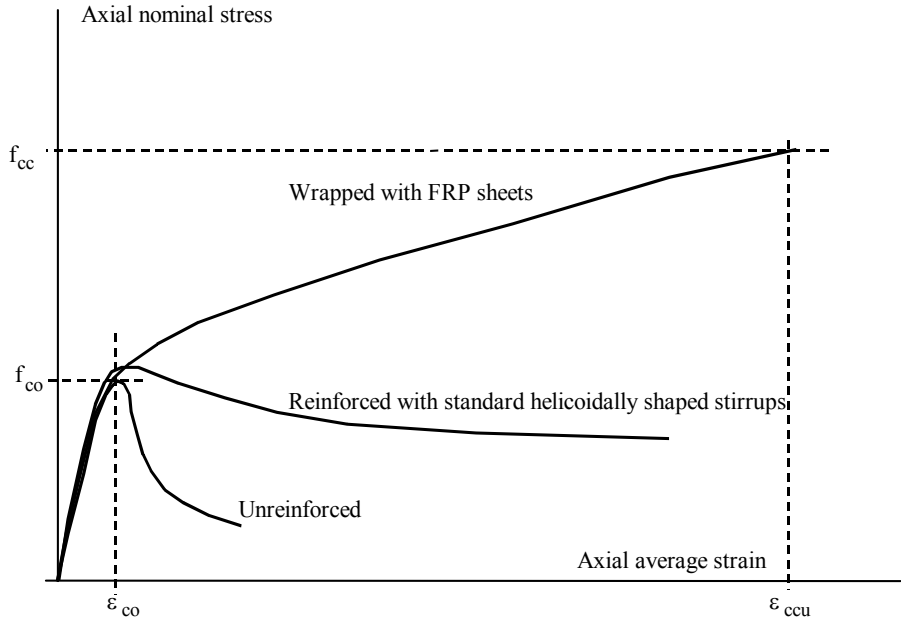

Fig. 1 Qualitative nominal stress vs. average strain curves in monoaxial compression for unreinforced, helicoidally shaped stirrups and fibrous composite sheets reinforced specimens.

Understanding the mechanism of transition from the strain-softening behaviour of unreinforced specimens to the monotone behaviour of wrapped specimens is fundamental to correctly predict the in load response of wrapped structural elements. In this paper, the transition is explained on the basis of a new interpretation of experimental data. A numerical simulation on compressed wrapped cylinders is provided to validate the new interpretation. To this aim, a new numerical code was previously developed[4], in which the only variable is the number of wrapping sheets.

EXPERIMENTAL BEHAVIOUR OF WRAPPED AND UNWRAPPED CYLINDERS

In the following, experimental results provided by Ghinelli[6] on wrapped concrete cylinders will be discussed. Compression tests were performed on unwrapped specimens and on specimens wrapped with one and three sheets of carbon (CFRP) and glass (GFRP) fibre composites. Specimens had a height of 30 cm and a diameter of 15 cm. Three specimens were tested for each type of lateral constraining. Axial stress, axial strain and circumferential strain have been acquired. In particular, the circumferential strain has been acquired by means of a steel chain, positioned on the middle cross-section (Fig. 2). The chain closure element was constituted by two springs, maintaining the chain in the right position. Between the two springs, a strain gauge has been positioned. Since the chain stiffness was much higher than the spring stiffness, it can be stated that the circumferential strain has been entirely charged by the two springs. The local measure provided by the strain gauge can thus be considered as representative of the circumferential strain on the middle cross-section.

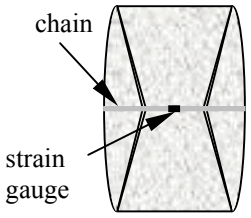

Fig. 2 Chain set-up for circumferential strain acquisition.

Said ε_l and ε_c, respectively, the axial strain and the circumferential strain, the volume strain ε_v is expressed as follows:

$$\varepsilon_v = \varepsilon_l + 2\varepsilon_c . \qquad (1)$$

The volume strain is considered as positive if involving volume decrement.
Named R the cylinder radius, the following relationship exists between ε_c and ε_r, the radial strain:

$$\varepsilon_c = \frac{2\pi\Delta R}{2\pi R} = \frac{\Delta R}{R} = \varepsilon_r . \qquad (2)$$

Since it is operatively difficult to acquire a radial strain directly, Eq. 2 has been used to indirectly acquire ε_r, as to identify the Poisson modulus ν through the known relationship for monoaxial loading:

$$\nu = -\frac{\varepsilon_r}{\varepsilon_l} . \qquad (3)$$

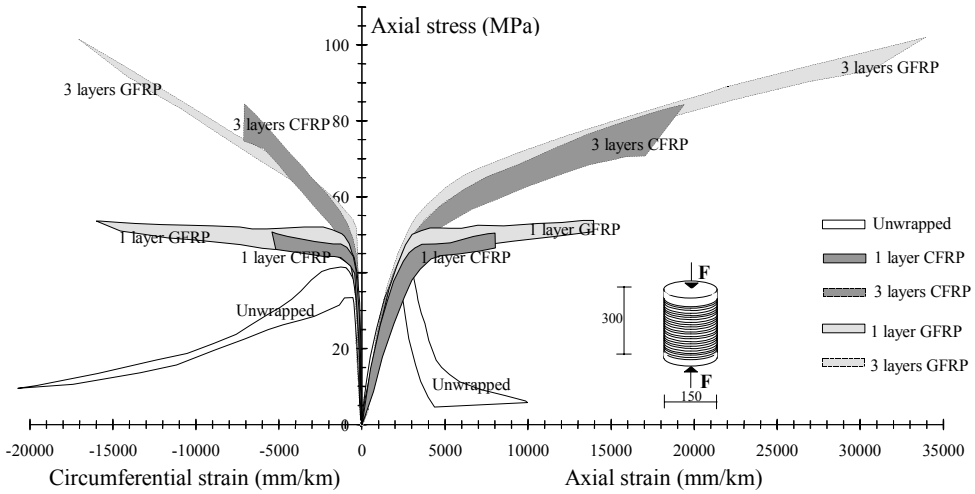

Fig. 3 Dispersion ranges of nominal stress vs. average strain curves, for unwrapped and wrapped specimens.

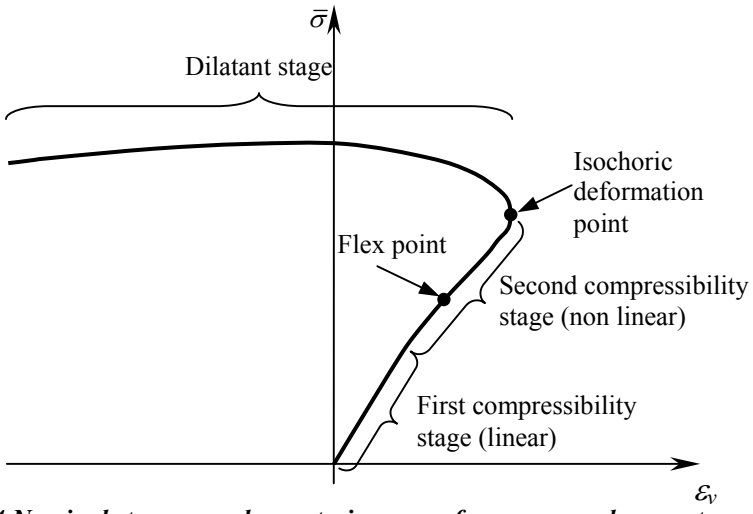

Fig. 4 Nominal stress vs. volume strain curves for unwrapped concrete specimens.

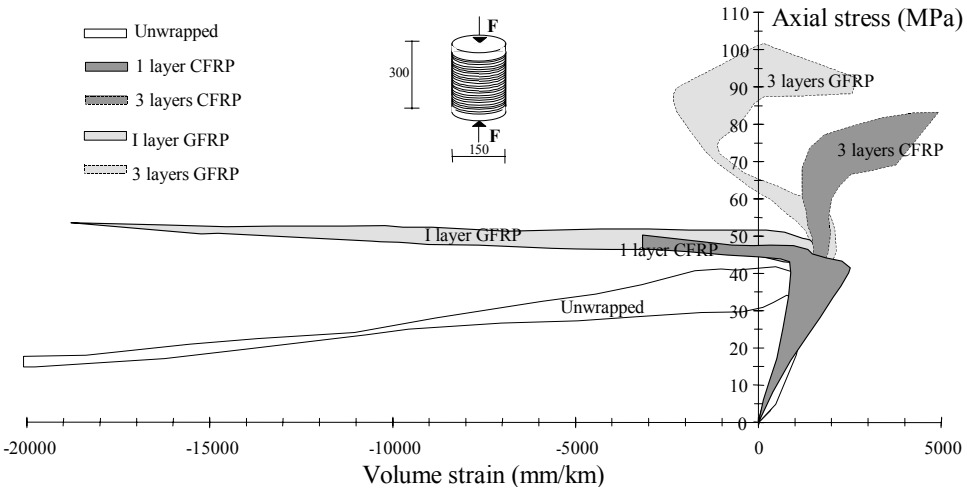

Fig. 5 Dispersion ranges of nominal stress vs. volume strain curves, for unwrapped and wrapped specimens.

In Fig. 3, the dispersion ranges of the nominal stress versus average strain curves are shown.

In unwrapped concrete specimens, the nominal stress versus volume strain curves for relatively low values of $\bar{\sigma}$ are linearly shaped[7] (Fig. 4). This first branch develops along the positive verse of the ε_v-axis and corresponds to a compressibility stage. It is followed by a non-linear branch, still developing along the positive verse of the ε_v-axis (Fig. 4), often showing a flex point. The standard approach interprets this further compressibility branch as a stage of micro-crack stable propagation. The second

compressibility branch ends when the curve tangent becomes infinite (Fig. 4). At this point, the minimum value of volume is reached and the deformation is isochoric, i.e., without volume variation. The standard approach interprets this point as the beginning of a crack instable propagation, with several micro-cracks coalescing into greater cracks. The following branch, developing along the negative verse of the ε_v-axis (Fig. 4), is viewed as a dilatant stage, due to the volume decrement for compressibility being opposed by crack openings. The dilatant and the two compressibility stages are considered to characterise the material behaviour for increasing loadings[7].

In the first compressibility stage, Eqs. 2 and 3 provide a Poisson modulus close to the static value. In the following two stages, the Poisson modulus becomes an increasing function of $\bar{\sigma}$. Unphysical values are rapidly reached, since the absolute value of the Poisson modulus exceeds 0.5 from the flex point forth.

In Fig. 5, the dispersion ranges of the nominal axial stress versus volume strain curves are shown for all the tested specimens. It can be seen that the dilatant behaviour gradually disappears with the application of FRP sheets. Harmon et al.[8] already found analogous volume curves.

STATE OF THE ART ON WRAPPED CONCRETE CYLINDERS MODELLING

As is well known, experimental data on concrete triaxial compressive tests (Fig. 6) are justified under the following assumptions[9]: -

- The ascending branch of the concrete compressive response describes concrete while it is undamaged;
- As the load increases, microcracks form within the concrete;
- The descending branch is not a material property, it depends on the manner in which the microcracks coalesce and on triaxial confinement of the concrete to restrain unstable crack propagation. In particular, hydrostatic pressure is seen largely to increase both maximum stress and maximum strain during compression, and the unstable strain-softening portion gradually vanishes for increasing pressures[10].

Several Authors have developed methods to predict the stress–strain ascending and descending parts of concrete subjected to triaxial compressive load. Among these, Ahmad and Shah[11] proposed an analytical stress–strain relationship depending on the three principal stresses and strains at the ultimate compressive strength. The five-parameter model of Willam and Waranke[12] allows obtaining the ultimate strength of concrete under combinations of multiaxial stresses. In particular, the strength envelope is defined using the uniaxial compressive strength, uniaxial tensile strength, strength under equal biaxial compression, high-compressive-stress point on the tensile meridian, and high-compressive-stress point on the compressive meridian. The modified hypoelastic model of Barzegar and Maddipudi[13] captures the behaviour under multiaxial loadings with good accuracy. The required parameters for calibration are uniaxial compressive strength, modulus of elasticity, and Poisson ratio.

Approaches for defining the concrete complicated stress–strain behaviour under various stress states can be divided in four main groups: -

1. Representation of given stress–strain curves by using curve-fitting methods, interpolation or mathematical functions;
2. Linear and non-linear elasticity theories;
3. Perfect and work-hardening plasticity theories;
4. Endochronic theory of plasticity.

When early tests on wrapped concrete were performed, the softening disappearance for increasing number of FRP sheets (Fig. 3) was explained on the base of the composite stiffness, very high in comparison with the concrete one. It was assumed that the wrapping provided confinement could substantially modify the structural element behaviour, which ceases to be softening and becomes hardening.

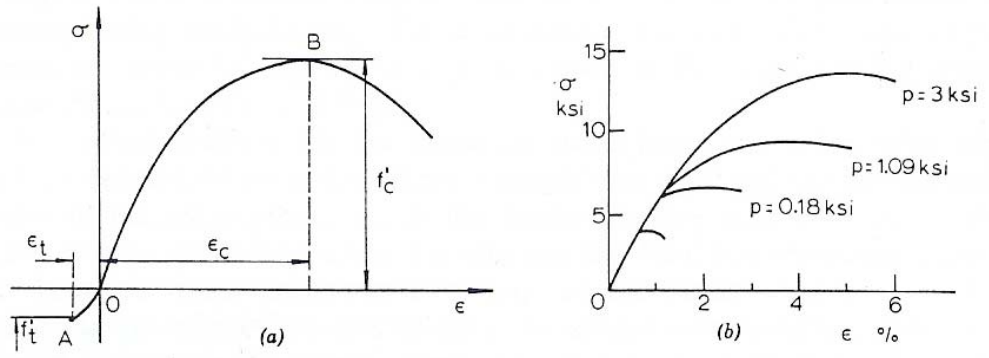

Fig. 6 Typical stress–strain curves for concrete under: a) uniaxial tension and compression; b) compression and lateral pressure (1 ksi=6.89 MN/M²).

As the attempt was made to numerically simulate the overall behaviour of wrapped elements starting from concrete and wrapping constitutive properties, separately considered, researchers were faced with a remarkable problem. By using the extended strain-softening relationship for concrete, it was not possible to reproduce the gradual softening disappearing for increasing confinement. Only strength increasing could be achieved. To avoid this problem, a modified concrete constitutive law was considered in simulations, depending upon the triaxial state of stress.

With the development of non-linear numerical tools for reinforced concrete structures analysis, the interest in the stress–strain behaviour of concrete has increased. Some of the main constitutive models used in the numerical analysis of reinforced concrete structures are listed below[10]: -

- Uniaxial and equivalent uniaxial models;
- Linear elastic-fracture models;
- Nonlinear elastic and variable moduli models;
- Elastic-perfectly plastic-fracture models;
- Elastic-strain hardening plastic and fracture models;
- Endochronic theory of plasticity for behaviour of concrete.

It was seen that existing models for confined concrete[11][14][15] are more appropriate for steel confined concrete than composite confined concrete. To adequately consider both the amount of confining stress and the level of radial strain, Harmon et al.[8] developed a mechanistic model for the stress-strain behaviour of confined concrete, which is based on the friction/dilatancy behaviour of concrete cracks. Directly related to the confinement effect of lateral reinforcement in columns are the concrete models of the following studies[16]: -

- Kent and Park[17]. The stress–strain model consists of a second-order parabola ascending branch and a straight line descending branch. The effects of confinement are reflected by adjusting the slope of the descending branch.
- Muguruma et al.[18] The model of the stress–strain curve is constructed by two second-order parabolas. The confinement effect is evaluated in terms of a confinement effectiveness coefficient. The evaluation method for the peak stress and the ultimate strain is based on a statistical study of test results.
- Sheikh and Uzumeri[19][20]. The stress–strain model reflects the confinement effect by adjusting the peak stress and a confinement effectiveness coefficient. The confinement effectiveness coefficient depends on the configuration of hoop reinforcement.
- Park et al.[21] The model of Kent and Park[17] is revised by introducing the increase in concrete strength caused by confinement. The confinement effect is proportional to the volumetric ratio and yield strength of hoop reinforcement. The deterioration rate of the falling branch is similar to that in the model of Sheikh and Uzumeri[19][20].
- Fujii et al.[22] The model consists of a second-order parabola and a third-order curve for the ascending branch. A confining effectiveness coefficient based on the model by Park et al. [21] is proposed. The peak stress and the deterioration rate are expressed as a linear function of the confinement effectiveness coefficient, based on a regression analysis of test result.
- Mander et al.[23][14]. A fractional expression to represent both the ascending and falling branches of the stress–strain curves is proposed. A confinement effectiveness coefficient for circular, square, and wall-type sections is introduced to evaluate the peak stress, on the base of a theory similar to the one by Sheikh and Uzumeri[19][20]. A constitutive model involving a specific ultimate strength surface for multiaxial compressive stresses is applied, which enables development of a theoretical model without dependence on a statistical analysis of test results.
- Razvi and Saatcioglu[24][25]. A parabolic ascending branch followed by a linear falling branch is proposed. The falling branch is a function of the strain corresponding to 85% of the peak stress.
- Hoshikuma et al.[16] A function of order *n* is used to represent the ascending branch, in which *n* is a constant to be determined from the boundary conditions. The falling branch is idealised by a straight line. The deterioration rate is developed from regression analysis of test data.

A review of the literature indicates that only few models for numerical analysis of reinforced concrete (RC) structures have been developed. As regards the effect on concrete confinement in RC tied columns, a proposal of 3D FE model has been provided by Xie et al.[26] in 1994. More recently, Barzegar and Maddipudi[27] proposed a 3D model for finite-element analysis of reinforced concrete based on the smeared cracking approach. One of the analytical estimations of the strengthening enhancement in wrapped columns is due to Richart[28]:

$$f_{cc} = f_{co} + 4.1\frac{f_{ft}t_f}{r}. \qquad (4)$$

In Eq. 4, f_{cc} is the compressive strength for wrapped concrete (Fig. 1), f_{co} is the compressive strength for unwrapped concrete, f_{ft} is the wrapping tensile strength, t_f is the wrapping thickness, and *r* is the specimen radius. The value of

the constant in Eq. 4 has been estimated previously by Considere and other researchers.
An experimental programme on wrapped and steel reinforced concrete columns is due to Mander[14]. It was observed that the confining effect varies on the specimen height for the non-uniform stirrups distribution. Moreover, in squared cross-section columns the confining effect concentrates in the corners. To take into account these two effects, two parameters k_1 and k_2 have been introduced for f_{cc} and ε_{ccu} evaluation:

$$f_{cc} = f_{co} + k_1 f_{fl}; \tag{5}$$

$$\varepsilon_{ccu} = \varepsilon_{co}\left(1 + k_2 \frac{f_{fl}}{f_{co}}\right). \tag{6}$$

Another approximated relationship has been proposed by Miyauchi et al.[29]. In this last relationship, a corrective factor k_e is added to Eq. 4:

$$f_{cc} = f_{co} + 4.1 \cdot k_e \frac{f_{fl} t_f}{r}. \tag{7}$$

On the base of experimental results, a value of k_e equal to 0.85 was identified.

CONCRETE CONSTITUTIVE MODEL

Discussion on strain-softening proper posedness: historical background

From the beginning of the 20th century forth, strain-softening has been widely regarded as inadmissible by several authors[30]. The first Author who considered strain-softening as an unacceptable feature for a constitutive equation was Hadamard[31]. He based his conclusions on the observation that the wave speed ceases to be real if the tangent modulus becomes negative. The problem of strain-softening in continuum dynamics has since been intensely debated at some conferences in regard to large-scale finite element computations[32]. It has been questioned[33][34][35] whether strain-softening in a continuum is a sound concept from the mathematical point of view. The question was whether or not strain-softening is a real material property or merely the result of inhomogeneous deformation caused by the experimental technique. A number of Authors have investigated the problem of "deformation trapping" from different standpoints[34]. In a study by Wu and Freud[36], the development of shear bands in a problem of wave propagation is examined by adopting a rate dependant model and conducting a boundary layer analysis. A similar approach has been proposed in a work by Sandler and Wright[35]. The common conclusion of these two studies is that the standard approach interpreting load–displacement experimental curves with softening as stress–strain does not lead to a meaningful representation of dynamic continuum problems in a physical and mathematical manner. In particular[35], the stability in the sense of Hadamard[31], i.e., proper posedness, is not satisfied, since in the softening regime the governing equation are elliptic instead of hyperbolic. Anyway, one can avoid the impossibility of constructing a time marching solution in dynamic continuum models of strain-softening with arbitrary initial conditions by simply introducing rate dependence. Sandler and Wright[35] proposed to add one term of rate-dependent viscoelastic behaviour to the standard rate-independent constitutive equation. This leads to stress–strain curves no more homothetic to the experimental load–displacement curves from which they are derived. The inclusion of rate dependence allows models with properly posed descriptions of strain-softening in dynamic continuum mechanics. Even though these models are stable in the sense of Hadamard (physically reasonable) they still manifest, in general, the physical instabilities always observed when strain-softening occurs.

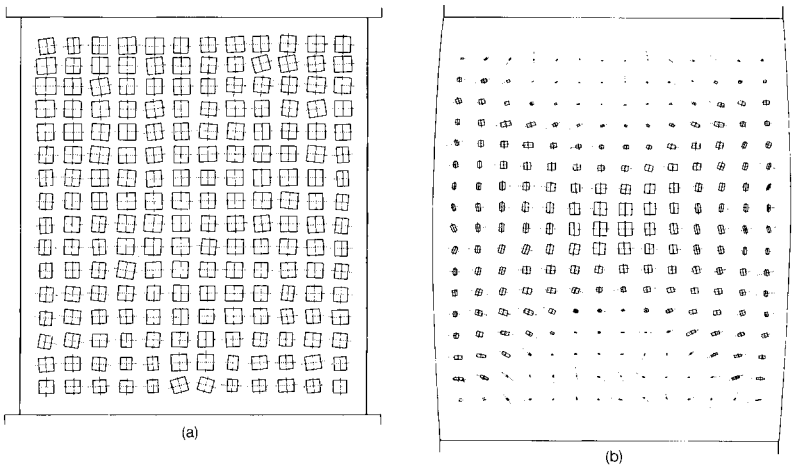

Fig. 7 Internal deformation field for dense sand; (a) lubricated end platens; (b) non-lubricated end platens (Deman, 1975).

1:1 specimen; 4-inch diameter

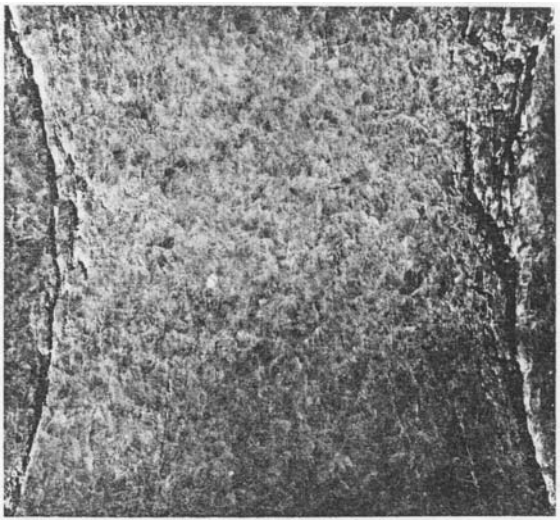

1/3:1 specimen; 4-inch diameter

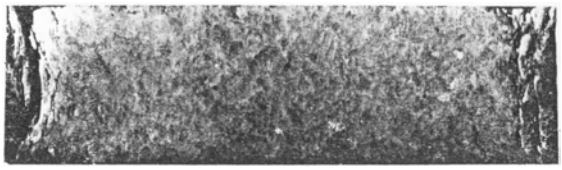

Fig. 8 Longitudinal section of Georgia Cherokee marble specimens at an advanced state of failure (Hudson et al., 1971).

It can be argued[34] that the formulation of localised deformation bands implies the non-validity of the usual assumption concerning homogeneous deformation and stress fields in the laboratory if strain-softening occurs. On the other hand, it is common knowledge that specimens in the strain-softening range of behaviour do not deform uniformly[37]. Kirkpatrick and Belshaw[38] and Deman[39] used an X-ray technique to investigate the strain field in cylindrical specimens of dry sand in triaxial compression tests with or without lubrication of the end platens. The non-lubricated case produces substantial non-homogeneous deformation, with the deformation being essentially confined to a wedge-shaped ring surrounding rigid cones adjacent to the end platens (Fig. 7). Lubrication prevents the formation of these cones (Fig. 7). The deformation is uniform for moderate strains, although bulging occurs at large strain.

Bishop and Green[40] came to similar conclusions by studying the influence of the slenderness of the specimen and the end friction.

Strain-softening in brittle materials such as rock and concrete can then be attributed to geometric effects that occur during laboratory testing and is not a material characteristic[34]. Thus, the conventional laboratory tests to determine material constitutive parameters are not appropriate in the presence of strain-softening. In this sense, the non-homothetic relationship between the experimental load–displacement and the Sandler-Wright stress–strain curves takes on a deeper meaning. It can then be concluded that some kind of non-linear relationship exists between the experimental load–displacement and the stress–strain curves, which non-necessarily has to be identified with a rate-dependent viscoelastic term, but surely leads to a substantial modification of the standard constitutive behaviour.

Numerous results from laboratory tests conducted with displacement control on rock and concrete under uniaxial compression and triaxial compression up to some critical confining pressure are available. In discussing the Hettler triaxial compression tests on flat specimens of dense dry sand[41], such as those of Deman[39], Dresher and Vardoulakis[42] concluded that softening in the triaxial test is mainly due to geometric effects and the commonly used slender specimens with non-lubricated end platens give an erroneous indication of the degree of material softening. The views of the test specimens of Hudston et al. in the advanced state of failure[43] exhibit gross slabbing of material, resulting in a decrease in the effective cross-sectional area (Fig. 8).

The $\sigma - \varepsilon$ curves obtained for these specimens by scaling the force by the original cross-sectional area rather than the continuously decreasing cross-sectional area show no softening for short specimens and a softening becoming increasingly prominent as the L/D ratio increases (Fig. 9).

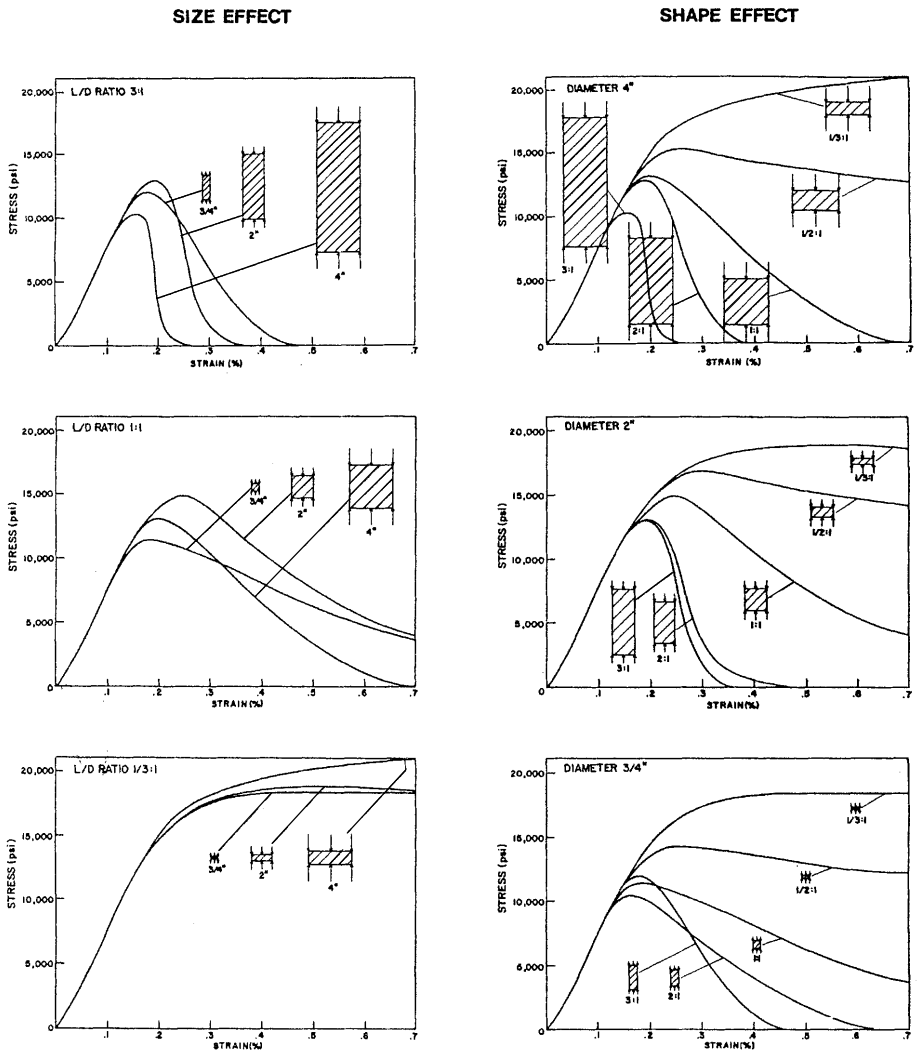

Fig. 9 Influence of specimen size and shape on the complete stress–strain curve for marble loaded in uniaxial compression (Hudson et al., 1971).

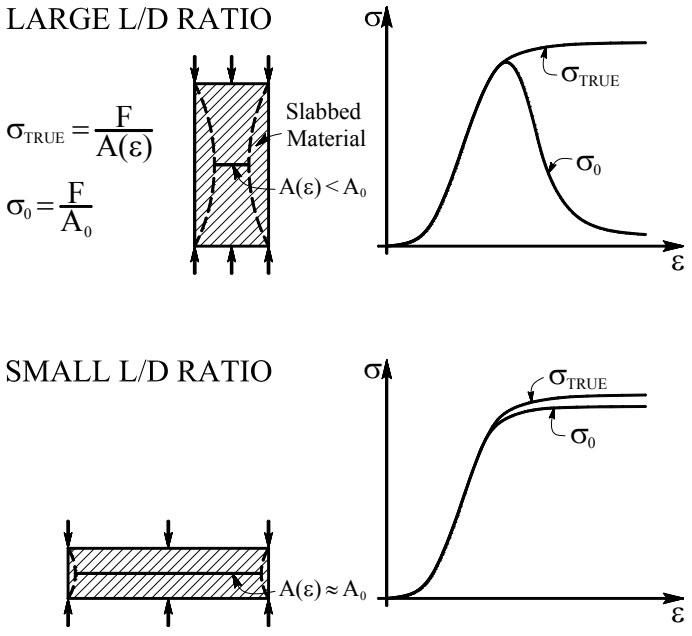

Fig. 10 Effect of stress definition on the shape of the stress–strain curve (Hudson et al., 1971).

On the basis of the views in Fig. 8, the significant effect which the L/D ratio exerts on the specimen response can be explained by reference to Fig. 10[43]: supposing that strain-softening is not a material property, but is essentially due to scaling the applied force by the original cross-sectional area rather than the actual cross-sectional area, for large L/D ratios the slabbing and shear failure lead to large reductions in the effective cross-sectional area and, then, to softening load–displacement curves, while for small L/D ratios the reduction in cross-sectional area is very small and load–displacement curves are still monotone non-decreasing.

The mentioned studies, even if all sharing the common idea of non constitutive nature of the softening behaviour, were not able to provide an identifying procedure from the experimental data to a monotone constitutive law for concrete. They only treated the problem under the theoretical point of view, since it was estimated[34] as extremely difficult, if not impossible, to experimentally track the effective cross-sectional area at each stage of the failure process. The impossibility to achieve a new constitutive proposal is the main reason for which this research field fell rapidly out of favour.

In 1985, Bažant[32] showed that strain-softening in a classical (local) continuum is not a mathematically meaningless concept. However, one can make the following remarks concerning this study, most of them emphasised by Bažant himself: -

- The closed-form solution is achieved only for certain boundary and initial conditions, and not for the general case;
- The stress in the strain-softening cross section is assumed to drop to zero instantly, regardless of the shape of the strain-softening diagram;
- The total energy dissipated in the strain-softening domain is assumed to vanish, while it is known that in strain-softening materials the dissipated energy assumes a finite value;
- The volume of the strain-softening is set to zero, while in strain-softening materials strain-softening regions of finite size are observed experimentally.

Moreover, Bažant pointed out that the parameters of the softening portion of the stress–strain diagram cannot be considered as characteristic properties of a classical continuum, since they have no effect on the solution. The justification provided by Bažant is that the length of the strain-softening region tends to localise into a point. In the opinion of the Authors of this study, the phenomenon has to be considered as a validation of the assumption of non-constitutive nature of strain-softening.

Nothing particularly worthwhile has been written on softening proper posedness since the mid-80's. The idea of non-constitutive nature of strain-softening was revived only several years later, in the Ph.D. Thesis of the first Author of this study[2]. This second time, theoretical considerations were supported by a new identification proposal for material properties. The results of this study will be presented in the following paragraph.

Monoaxial identification

In this study, the effective law proposed by Ferretti in 2001[2] has been adopted to describe the constitutive behaviour of concrete in monoaxial compressive loading. The starting point of this proposal is the non-objectiveness of the standard approach in front of the size-effect, together with the question of whether or not it is possible to associate a physical meaning with the concept of instability in the infinitesimal neighbourhood of a point. The observation that a constitutive law should not exhibit a size-effect puts a serious doubt on the validity of the standard approach. The physical meaningless of instability in the infinitesimal neighbourhood of a point puts a more serious doubt on the constitutive nature of strain-softening.

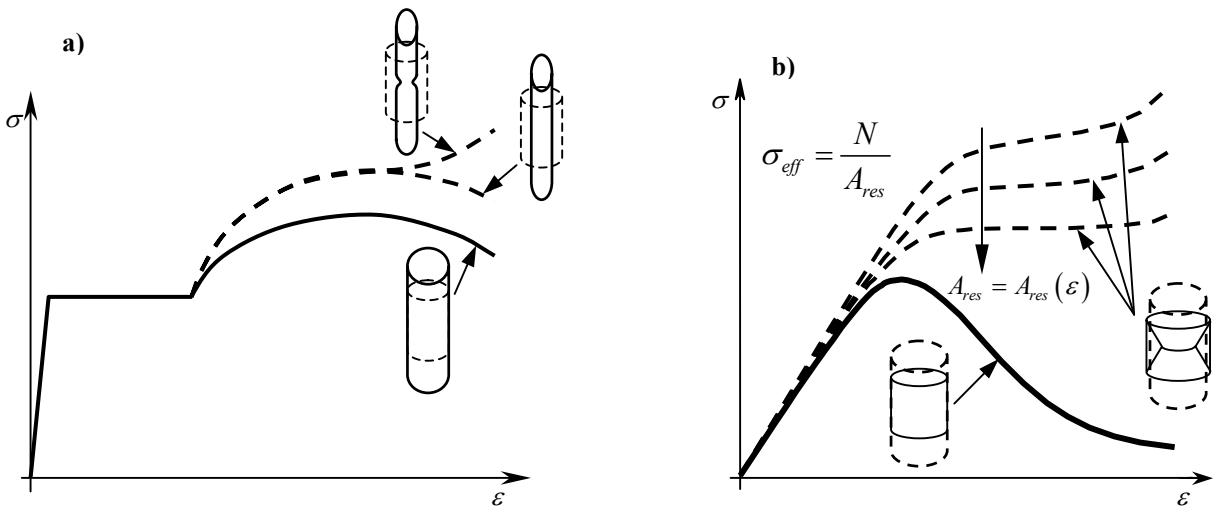

Fig. 11 Stress identification from load data: influence of the middle cross-section evaluation for steel (a) and concrete (b).

It seems therefore reasonable to assume that strain-softening is not a material property and the true constitutive behaviour, named the "effective behaviour", admits the qualitative representation shown with dashed line in Fig. 11.b, quite equivalent to Fig. 10.

Similar argumentations on the implications of failure mechanism (Fig. 8) on specimen response as those of Hudson et al.[43] have inspired the new proposal. Once again, it was assumed that strain-softening is due to scaling the applied force by the original cross-sectional area rather than the actual cross-sectional area, named the "resistant area" A_{res} (Fig. 11.b), as happens with steel (Fig. 11.a). Since the resistant area decrement is an internal not observable mechanism in concrete, the function $A_{res} = A_{res}(\varepsilon)$ is not directly measurable and has to be identified. InFig. 11.b, qualitative effective laws are provided for three different assumptions on A_{res}.

The non-objectiveness of the standard approach has been imputed to the impossibility of performing mechanical tests on the material directly: the object in testing is never the material, but a small structure interacting with the test-machine. Thus, experimental results univocally characterise the behaviour of the specimen-test machine system, while they are not at all representative of the constitutive behaviour. Also the softening branch has a meaning linked to a structural property: structural instability. This branch cannot provide any information on the constitutive behaviour, except through an identifying model.

To redefine the identification model allowing us to derive constitutive properties from experimental data, it is necessary to evaluate all the factors influencing a test result *R*, the known output of our identifying problem with unknown inputs (Fig. 12). Among these inputs, there is the constitutive behaviour *C*, which is unknown in value. The other contributions are unknown also in kind and number. The knowledge of *f*, the function relating *R* to all the unknown inputs, is fundamental to establish a relationship between *R* and *C*, the input to identify. The *C* identification places then as a typical inverse problem. As most of the inputs are unknown in kind and number, the definition of a model is required to establish the correlation between *C* and *R*.

In the model here adopted it has been assumed that the main factors influencing *R* are four: constitutive properties (*C*), structural mechanics (*S*), interactions between test-machine and specimen (*I*), and test-machine metrological characteristics (*M*). A qualitative representation of the four factors for three different load-steps is shown in Fig. 13.

Fig. 13 shows that the four factors are load-step functions. Then, it is not possible to establish a proportional ratio between structural and material behaviour. That is to say, the load–displacement and stress–strain diagrams are not homothetic (Fig. 14).

Said $\bar{\varepsilon}$ the average strain and defined the effective stress σ_{eff} as shown in Fig. 11.b, it was analytically demonstrated[2] that the derivative $d\sigma_{eff}/d\bar{\varepsilon}$ has to be strictly positive until $\boldsymbol{Q}$, the point corresponding to $\boldsymbol{P} \equiv (\hat{v}, N_{\max})$ (Fig. 15). The $d\sigma_{eff}/d\bar{\varepsilon}$ sign for $v > \hat{v}$ is not univocally determinable by algebraic considerations, since it depends on the failure path.

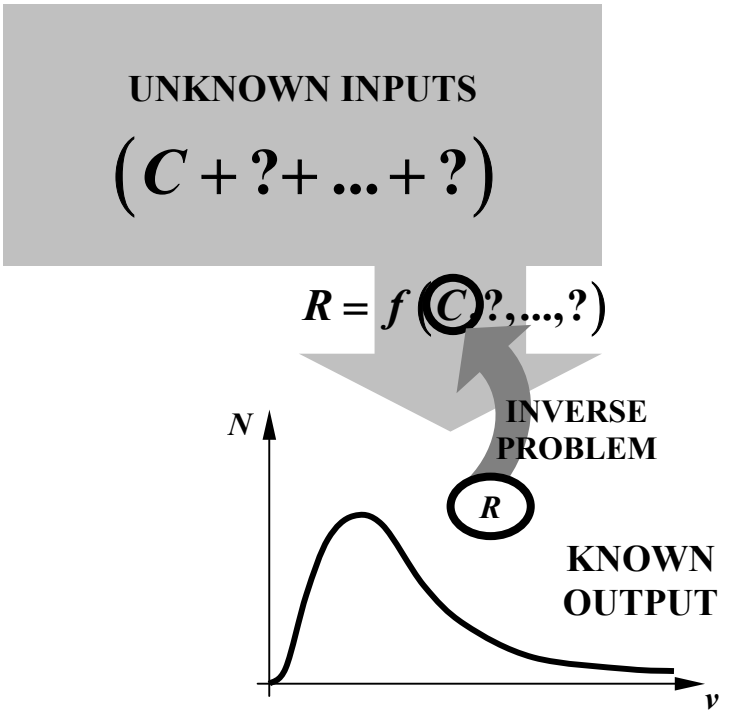

Fig. 12 Schematisation of an experimental test: compression case.

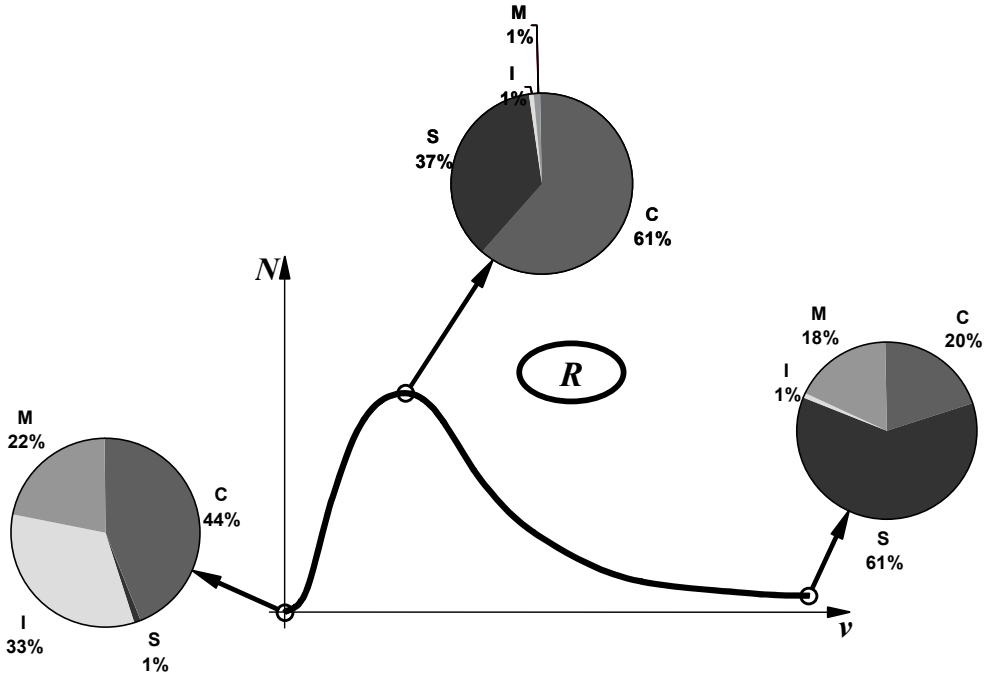

Fig. 13 Factors influencing a test result for three different load-steps.

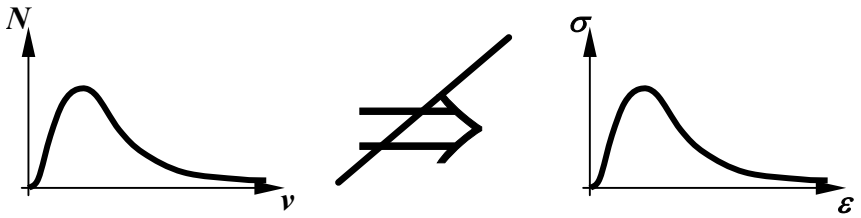

Fig. 14 New approach for stress–strain identification.

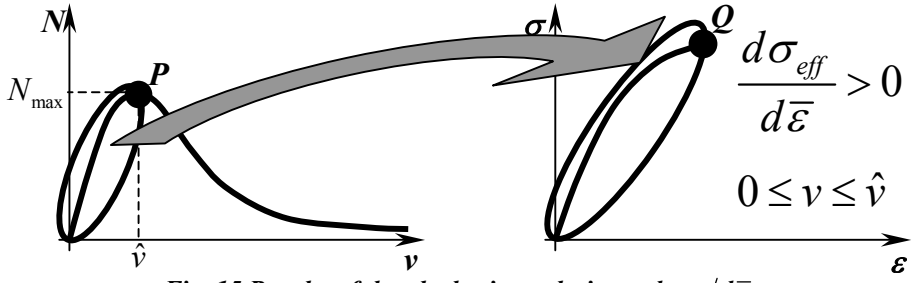

Fig. 15 Results of the algebraic analysis on $d\sigma_{eff}/d\bar{\varepsilon}$.

Fig. 13 clearly shows that the main factor among the non-constitutive ones is *S*, except for the incoming failure stage. *S* regulates the modification of the specimen resistant structure, through the development of a failure mechanism. The specimen has been assumed to fail with propagation of a dominant crack, as shown in Fig. 2. The outer part of the specimen loses its capability to carry load as the dominant crack propagates, while the inner part of the specimen, the one termed "the internal core", is able to carry load even when the dominant crack has finished propagating. The law of the resistant area A_{res} takes into account the variation of resistant structure. A_{res} depends on the value of the minimum cross section area and on the contribution of the adjacent material.

It was proposed to estimate A_{res} in accordance with the Fracture Mechanics with Damage, by assuming a scalar value for the damage parameter *D*:

$$A_{res} = A_n\left(1-D\right). \tag{8}$$

To evaluate $D = D(R)$, two experimental damage laws were employed. The first damage law, D_1 [44], relates damage to the microseismic signal velocity at the current point, *V*, and the initial microseismic signal velocity, V_0 :

$$D_1 = 1 - \frac{V}{V_0}. \qquad (9)$$

The second damage law, D_2 [1][2], relates the damage to the dissipated energy at the current point, W_d, and the total dissipated energy, $W_{d,t}$:

$$D_2 = \frac{W_d}{W_{d,t}}. \qquad (10)$$

The evaluation of W_d has been done in accordance with the experimental unloading-reloading law.

D_1 and D_2 turned out to be very close to each other. Damage laws were experimentally derived for variable specimen slenderness. Fig. 16 shows D_2 damage laws obtained for H/R ratios varying from 3 and 8. As can be appreciated, damage laws are size-effect sensitive. That is, the highest is the H/R ratio, the highest is D_2 at each load-step.

The identifying procedure for the effective strain, ε_{eff}, is based on the identified value of σ_{eff} and the slope of the unloading-reloading cycle at the current point, as shown in Fig. 17.

Load–displacement diagrams, $N - v$, for the specimens of the experimental programme[2] are shown in Fig. 18. The size-effect in the $N - v$ plane involves a decrement of both the tangent to the origin and the maximum load with the increasing of the $H - R$ ratio.

The $\sigma_{eff} - \varepsilon_{eff}$ relationships obtained for the six tested geometries fall within the dispersion range in Fig. 19. The average curve in Fig. 19 is actually monotone non-decreasing, as was expected from the preventive theoretical analysis (Fig. 11.b). This is a notable result, since the monotonicity of the effective law has not been assumed a-priori, but has been obtained directly from experimental data, scaling the applied load by the experimentally evaluated resistant area.

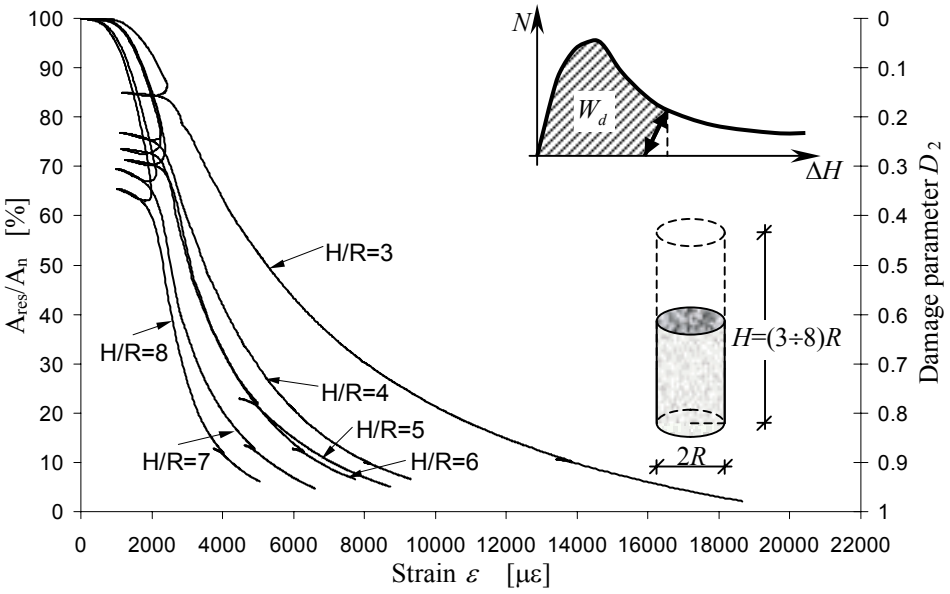

Fig. 16 Evolution of resistant area and D_2 damage law for variable slenderness.

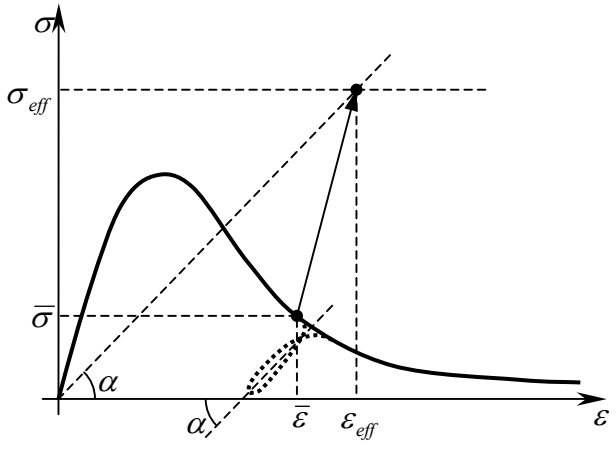

Fig. 17 Identification of ε_{eff} starting from the known value of σ_{eff}.

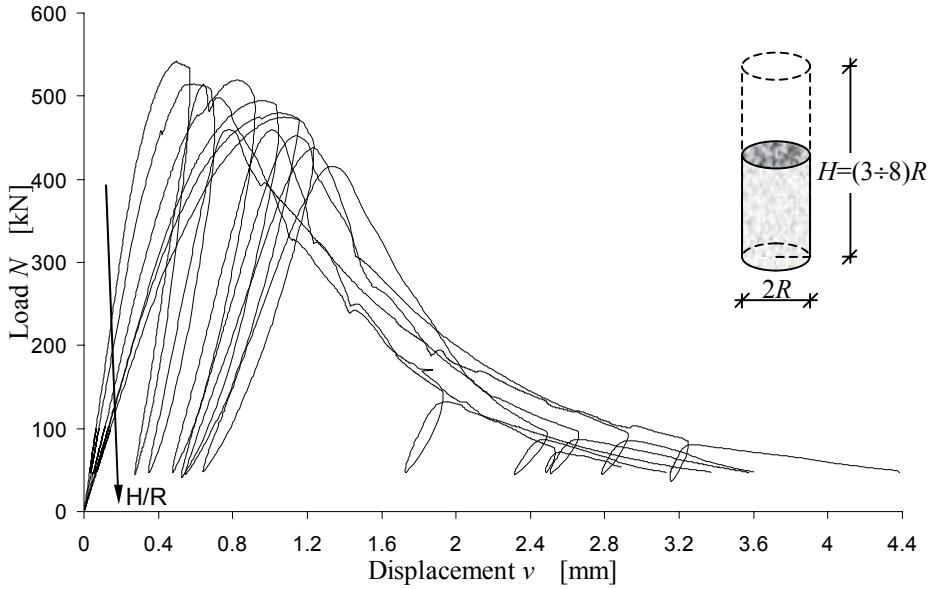

Fig. 18 Size effect for the load-displacement diagrams.

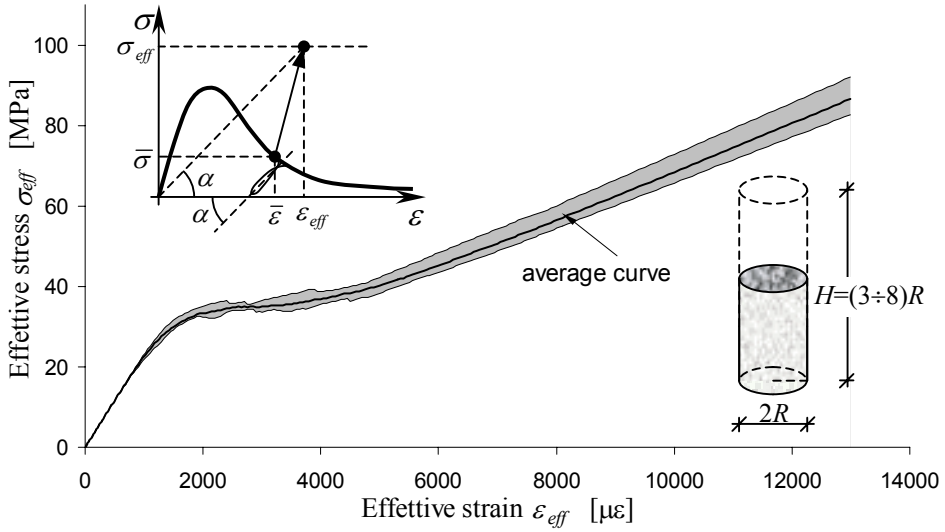

Fig. 19 $\sigma_{eff} - \varepsilon_{eff}$ dispersion range for variable slenderness and average curve.

Since the dispersion range is very narrow, it can be stated that the $\sigma_{eff} - \varepsilon_{eff}$ curves are size-effect insensitive. It can also be shown[3] that the identified curve is not sensitive to changes of failure mechanism.

An important consequence of the failure mechanism with dominant crack is that strain measurements on the cylindrical specimen surface cannot be employed to evaluate the Poisson ratio. As shown in Fig. 2, from the dominant crack initiation forth the circumferential strain acquisition is indeed affected by crack openings. Once more, experimental acquisition is something related to the specimen and not to the material behaviour. From the crack initiation forth, then, Eq. 3 can be no longer used in conjunction with Eq. 2 to identify the Poisson modulus. This gives an explanation to the unphysical Poisson modulus identified by means of the middle cross-section strain-gauge[6][2] (Fig. 20). Those values no longer pose a problem, since they do not actually represent a Poisson modulus.

To verify this assertion, a radial strain acquisition was performed[2] into the resistant core of unwrapped specimens, by means of fibre optic sensors (FOSs). The $\varepsilon_r / \varepsilon_l$ ratio for this new acquisition is almost constant with ε_l (Fig. 20). Since it was assumed that macro-cracks do not occur in the resistant structure, the $\varepsilon_r / \varepsilon_l$ constant behaviour could be considered more representative of the Poisson ratio ν than the increasing behaviour is.

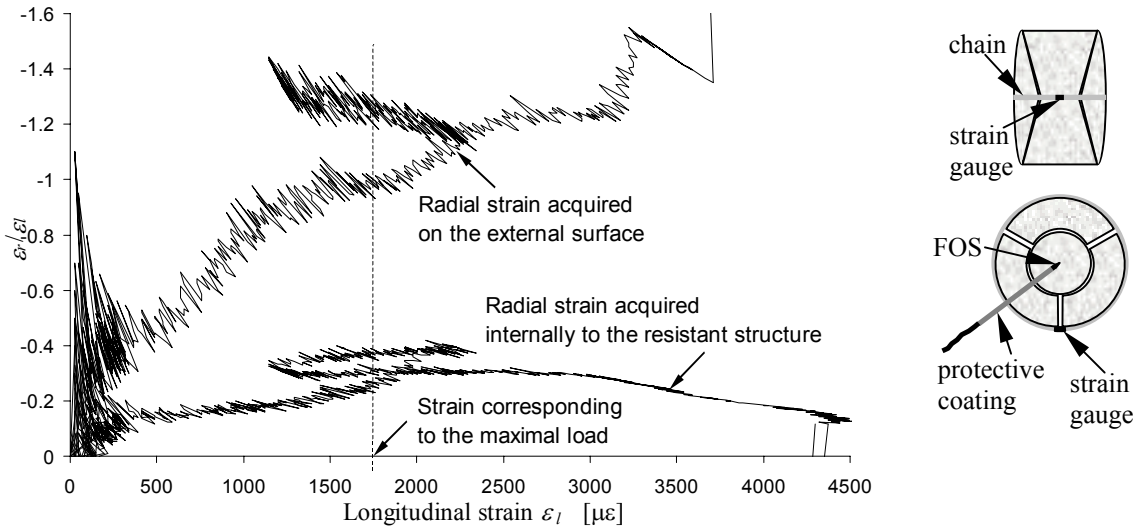

Fig. 20 Traditional and identified $\varepsilon_r/\varepsilon_l$ ratios.

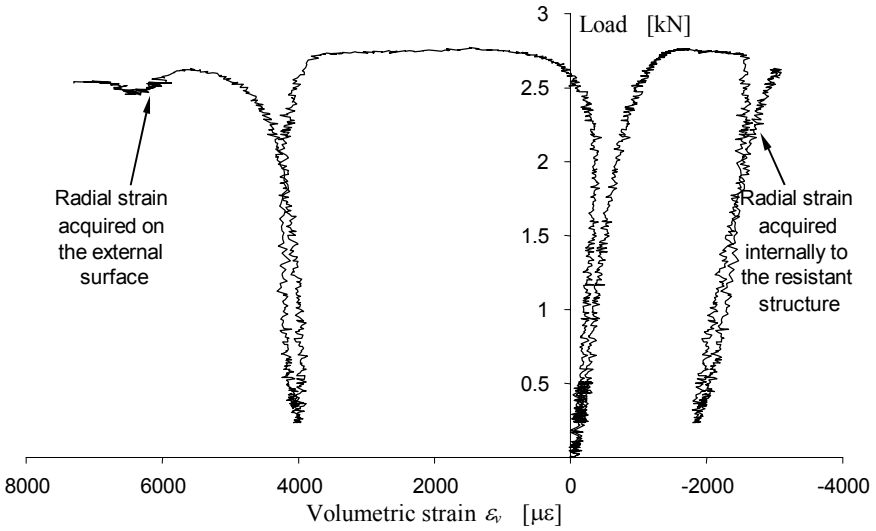

Fig. 21 Traditional and identified volume curves.

Finally, the new volume curve integrally belongs to the negative field (Fig. 21). Contrarily to what has been asserted traditionally[7], then, concrete never exhibits a dilatant behaviour. Volume increasing was already imputed to shear dilatancy by Harmon et al.[8], but it was still considered as a material property. Now, dilatancy is directly connected to the failure mechanism and, then, to a structural property. The volume increasing itself is considered as a structural property. Acquisitions in the internal resistant core (Fig. 20 and Fig. 21) validate this assumption.

Triaxial model

For the adopted monoaxial identification model, unloading-reloading cycles in the $\sigma_{eff} - \varepsilon_{eff}$ plane are lines passing through the origin. The instantaneous constitutive behaviour can then be considered as linear elastic, with the instantaneous Young's modulus given by the secant modulus. Since compressive tests were performed under quasi-static conditions, each load-step corresponds to an equilibrium stage, in which the Hooke's laws are valid:

$$\underset{\sim}{\varepsilon} = \underset{\sim}{C}\underset{\sim}{\sigma} \qquad (11)$$

Eq. 11 represents the triaxial extension of the monoaxial effective curve in Fig. 19, at the general load step.

CONCRETE-FRP INTERFACE MODELLING

Compressive-tests results on wrapped and unwrapped concrete cylindrical specimens are schematised in Fig. 22, for the case of carbon fibre wrapping (CFRP). It can be seen that the load–displacement experimental curves for the wrapped and the unwrapped specimens are more or less superimposed until the value of platens relative displacement $\tilde{v}$.

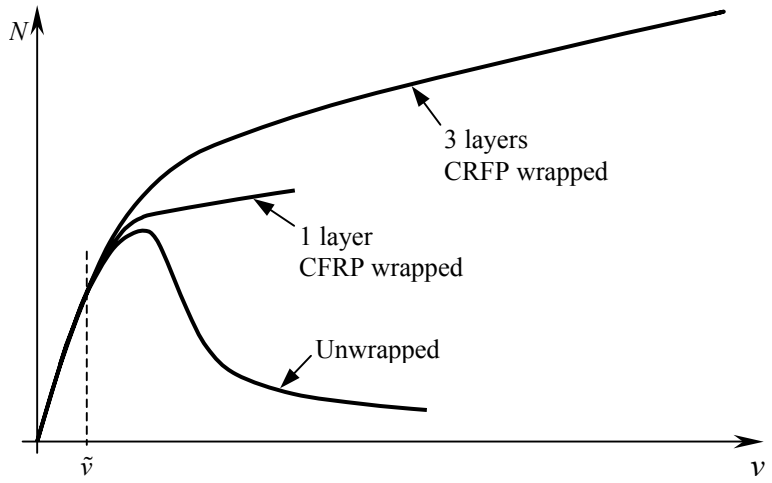

Fig. 22 Load–displacement curves for unwrapped, one layer CFRP wrapped and three layers CFRP wrapped specimens (schematic representation).

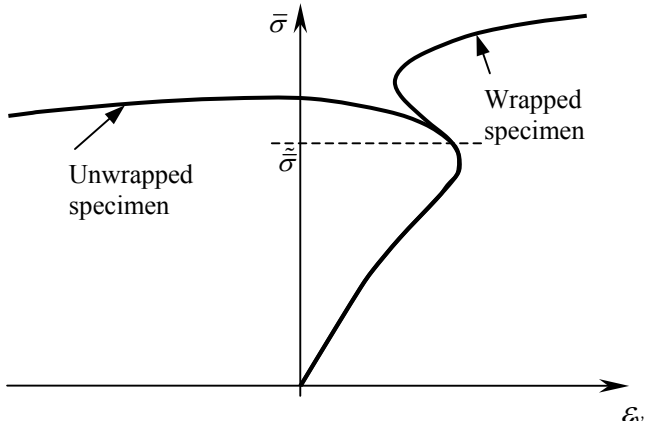

Fig. 23 Volume curves for wrapped and unwrapped specimens (schematic representation): for the adopted convention, the values of volume strain on the positive axis are negative.

Also the volume curves are more or less superimposed until $\tilde{\bar{\sigma}}$, the average stress corresponding to the relative displacement $\tilde{v}$ (Fig. 23). It can then be concluded that wrapping does not work for $v < \tilde{v}$.

For $v \geq \tilde{v}$, the influence of the wrapping becomes more and more sensitive. This leads to greater value of load supported by the specimen in comparison to the unwrapped case, and to the disappearance of the softening behaviour in the load–displacement curves (Fig. 22). As concerns the volume curves, the wrapping influence for $\bar{\sigma} \geq \tilde{\bar{\sigma}}$ leads to the disappearance of the dilatant behaviour observed in the unwrapped specimens[6][8] (Fig. 23).

To take into account the experimental behaviour, the interface between concrete and FRP wrapping has been modelled by means of the relationship drawn in Fig. 24, where ν is the Poisson Modulus, ε_t and σ_t are, respectively, the strain and the stress in the transversal direction, and $\tilde{\varepsilon}$ is defined as follows:

$$\tilde{\varepsilon} = \frac{\tilde{v}}{h}. \qquad (12)$$

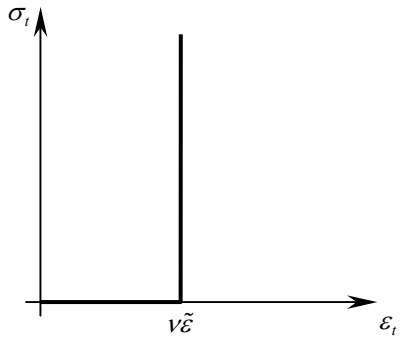

Fig. 24 Adopted model for concrete–FRP wrapping interface.

In Eq. 12, h is the specimen height. The interface is then assumed to be infinitely deformable for $\varepsilon_t < \nu\hat{\varepsilon}$ and infinitely rigid for $\varepsilon_t \geq \nu\hat{\varepsilon}$.

NUMERICAL MODEL

Generalities on the Cell Method (CM) code

The numerical analysis has been performed by means of the Cell Method (CM), using the numerical code developed by Ferretti[4]. The CM

divides the domain by means of two cell complexes, in such a way that every cell of the first cell complex, which is a simplicial complex, contains one, and one only, node of the other cell complex. In this study, a Delaunay/Voronoi mesh generator is used to generate the two meshes in two-dimensional domains. The primal mesh (the Delaunay mesh) is obtained by subdividing the domain into triangles, so that for each triangle of the triangulation the circumcircle of that triangle is empty of all other sites (Fig. 25). The dual mesh (the Voronoi mesh) is formed by the polygons whose vertexes are at the circumcenters of the primal mesh (Fig. 25). For each *Voronoi* site, every point in the region around that site is closer to that site than to any of the other Voronoi sites. The conservation law is enforced on the dual polygon of every primal vertex.

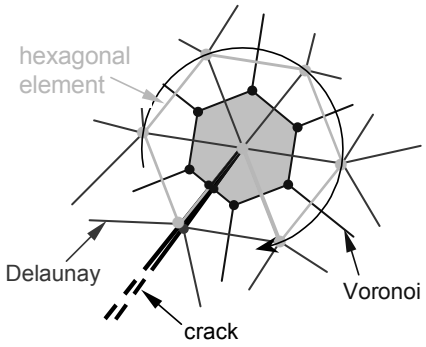

Fig. 25 Hexagonal element for analysis in the Mohr-Coulomb plane.

To identify the Mohr's circle for the tip neighbourhood, a hexagonal element was inserted at the tip[4] (Fig. 25). When the mesh generator is activated, the hexagonal element is divided into equilateral Delaunay triangles and a quasi-regular tip Voronoi cell is generated (the cell filled in grey in Fig. 25). This allows us to establish a correspondence between the tip stress field and the attitudes corresponding to the sites of the tip Voronoi cell. It has been shown[4] that the tension points correctly describe the Mohr's circle in the Mohr-Coulomb plane, for each rotation of the hexagonal element around the tip. The propagation direction is then derived as the direction of the line joining the tangent point to the Mohr's pole (Fig. 26).

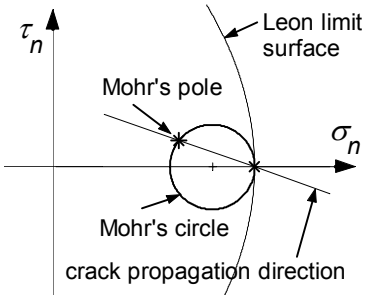

Fig. 26 Leon limit surface in the Mohr-Coulomb plane.

Once the limiting load has been reached, the specimen geometry is uploaded through a combination of nodal relaxation with intra-element propagation and remeshing[4]. It is then possible to reproduce the crack path development from enucleation to the final stage.

Tool for Mixed-Mode analysis

The compressive test on cylindrical specimens is a typical example of mixed mode loading. Mixed-mode crack propagation occurs whenever the load is applied obliquely to the crack direction and the crack opening direction (Fig. 27).

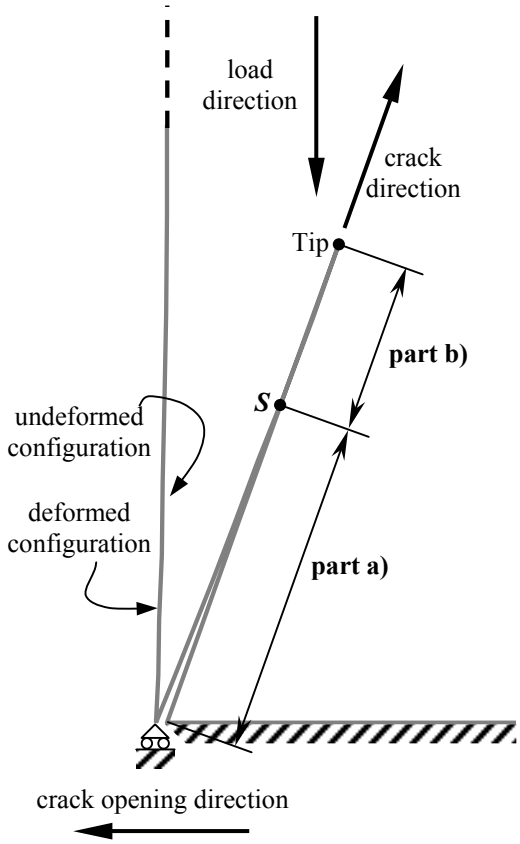

Fig. 27 Mixed-mode crack loading.

When subjected to mixed-mode loading, a crack can be divided into two parts[2]:

part a) Mode I prevails and the two edges of the crack separate;

part b) Mode II prevails and the two edges of the crack slide over one another.

Numerical simulation is only possible if the position of the point ***S*** separating the two parts is known. The dominance of Mode I rather than Mode II crack propagation involves different boundary conditions on the crack surfaces, and it is necessary to specify every boundary condition before the simulation starts. In general, ***S*** is a function of the load step and crack length, and is, thus, an unknown of the mixed-mode problem. To determine ***S***, it is necessary to proceed step-wise:

Step I) Evaluate the deformed configuration of the domain, by assuming free displacement all over the crack (giving the step I deformed configuration);

Step II) Use the step I deformed configuration to find the part b) extension, by assuming zero relative displacement between opposing nodes lying in part b) (giving the step II deformed configuration);

Step III) Introduce relative displacement between the opposite nodes lying in part b), and re-evaluate the extension of part b) (giving the final deformed configuration).

Step III involves introducing FEM contact elements describing sliding contact[45][46][47].

A more detailed description of the steps necessary to determine the position of ***S*** follows.

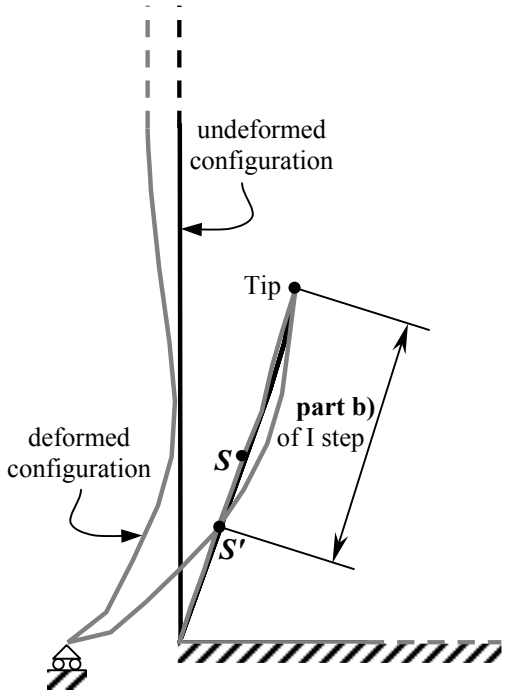

Fig. 28 Crack deformed configuration after Step I.

In the first step (Fig. 28), all nodes lying on the crack are free to move, independent of any displacement constraint relative to the opposite crack edge. Hence, no force acts on the nodes lying on the crack. In part b), this involves penetration of the nodes below the opposite crack surface. Depending upon the geometry of the domain, and the boundary conditions, it is also possible that some nodes lying in the part a) may penetrate below the opposite crack surface. Thus, the point ***S′*** separating the part a) and the part b) portions of the crack does not generally coincide with ***S*** after Step I. The position of the point ***S′*** defines the extent of part b) after step I.

During the second step, the penetration is eliminated, and the extent of part b) adjusted. A special tool has been developed to eliminate the penetration of nodes between crack surfaces. This tool examines all the nodes along the same surface of the crack lying in part b) after step I, starting from the tip. At each node, the program checks to see whether penetration occurs. If this is the case, the current node is constrained to have the same displacement components of the opposite node on the crack.

By specifying equal displacements to the nodes on either side of the crack, a constraint in correspondence of the current node is introduced. The reaction forces due to the imposed constraint are applied to the opposite node by change of their sign. These applied forces cause the opposite surface of the crack to deform and, thus, affect the displacement components of the opposite node. To ensure that the paired nodes have the same displacement components (and to re-assess the constraint reactions), the displacement components of the current node must be adjusted until a stable solution is reached. Every time the boundary conditions of a crack node are changed, the tool re-evaluates the extent of part b), and re-examines all the nodes lying in part b), starting from the tip. Each change in boundary conditions involves a change in the extent of part b), and hence a change in the number of nodes lying in part b).

After changing the boundary conditions of a general node lying in part b), it is possible that a node that has previously been examined may become subject to tensile stress. The constraint at this node may no longer be required, due to the introduction of a new constraint at the current node.

For this reason, after re-evaluating the extent of part b) the tool controls whether a node is in traction. If so, deformation constraint at the nodes in tension are relaxed and the extent of part b) is re-evaluated.

Step II gives a deformed configuration that clearly shows the subdivision of the crack into part a) and part b). The point separating these two parts, ***S″***, is not yet the actual point ***S***, as it does not consider the slip between opposite nodes lying in part b).

Step III estimates the components of relative slip between opposite nodes lying in part b).

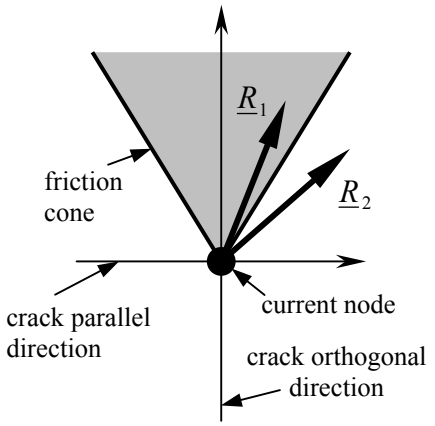

Fig. 29 Example of the validity ($\underline{R}_1$) and of non-validity ($\underline{R}_2$) of the no relative slip assumption.

A friction model is used to assess the forces acting across the crack surfaces. The friction coefficient is assumed to be independent of the amount of slip and the value of the normal force. Relative slip can only take place if the constraining reaction forces for nodes in part b) lie on the surface of the friction cone (Fig. 29).

In Fig. 29, $\underline{R}_1$ is a constraint reaction that lies inside the friction cone. For this case, the constraint condition adopted for the current node in step II is correct and no relative slip occurs between it and the node on the opposite crack surface. $\underline{R}_2$ is a constraint reaction that lies outside the friction cone. In the adopted model, reactions lying outside the friction cone cannot exist. Thus, the constraint condition adopted at the current node in step II is not correct, and relative slip will occur between it and the node on the opposite crack surface. The correct value of relative slip results in a reaction that lies upon the conical surface. The following steps are used to estimate the value of relative slip: -

- An assumed slip is considered at the current node (the first approximation relative slip).
- The new constraining reaction force is evaluated (giving the second approximation of constraining reaction force).
- If the second approximation constraining reaction force lies outside the friction cone, the first approximation relative slip is smaller than the actual slip. Thus, the relative slip is doubled (giving the second approximation relative slip).
- If the second approximation constraining reaction force lies within the friction cone, the first approximation relative slip is greater than the actual slip. Thus, the relative slip is halved (giving the second approximation relative slip).
- The preceding steps establish upper and lower bounds on the relative slip. Interval halving is used to determine the correct slip, for which the upper and lower bounds are equal (to within a particular tolerance).

The common value of the upper and lower bounds is used as the actual value of relative slip.

The node with the maximum angle between the constraining reaction force and the normal to the crack surface is considered first when calculating the relative slip. When relative slip is introduced at the current node, the constraint reactions force at the other nodes will change. Three cases can occur:

1. A constrained node may become subject to tension;
2. A constraint reaction may move to outside from the friction cone;
3. A node lying in part a) during step II may penetrate the opposite crack surface.

Each time a value of relative slip is calculated, the tool checks whether one of these cases has occurred. If this is the case, the process is repeated with the appropriate modifications. In subsequent iterations, the tool remembers the relative slips that have previously occurred along the crack: the same relative slip is maintained between the nodes in part b), so long as the constraint reaction force does not move to outside the friction cone. This allows the energy dissipation associated with each value of relative slip to be estimated.

Finally, the tool also remembers the relative displacements between nodes in part a). In particular, it remembers the relative displacements in the crack direction. If a node lies within part a) for a given imposed displacement, and lies in part b) for the next value of imposed displacement, the relative displacement in the direction normal to the crack surface goes to zero, while the relative displacement in the direction of the crack does not change. Thus, the assumption of zero relative slip during step II may be very far from the truth. Consequently, the simulation may not converge. The tool avoids this problem by modifying the step II constraint conditions for all iterations after the first. Nodes that penetrate the opposite crack surface are constrained to have the same displacement component in normal to the crack surface and to dist in the crack direction by the same relative displacement as in the previous iteration.

Estimation of the confining pressure

Said $d_{\max}$ the maximal radial displacement for which the wrapping does not work, the specimen behaves as if no wrapping is applied on the surface until the deformed middle cross-section circumference, c, is less-equal than $c_{\max}$, defined as follows:

$$c_{\max} = 2\pi\left(r + d_{\max}\right). \qquad (13)$$

The quantity $2\pi\left(r + d_{\max}\right)$ is representative of the wrapping initial length, assumed to be slightly greater than the circumference of the specimen. This assumption is consistent with the technique currently employed for wrapping.

For $c > c_{\max}$, the wrapping starts to deform with a strain ε equal to:

$$\varepsilon = \frac{2\pi\left(r' - r - d_{\max}\right)}{2\pi\left(r + d_{\max}\right)} = \frac{U - d_{\max}}{r + d_{\max}}. \qquad (14)$$

In Eq. 14, r is the initial cylinder radius, r' the cylinder radius in the deformed configuration, and U the absolute value of radial displacement for the middle cross-section. The strain is positive valued, since it corresponds to fibre extension. The correlated tensile stress is equal to:

$$\sigma = E_f \frac{U - d_{\max}}{r + d_{\max}}. \qquad (15)$$

In Eq. 15, E_f represents the Young's modulus of the FRP wrapping.
Internal and external forces acting on an FRP strip of unit height are shown in Fig. 30, where σ_{rc} is the radial stress provided by the concrete cylinder to the FRP strip, and F_f is the resultant of the tensile stresses acting on the FRP strip of unit height and thickness *s*.

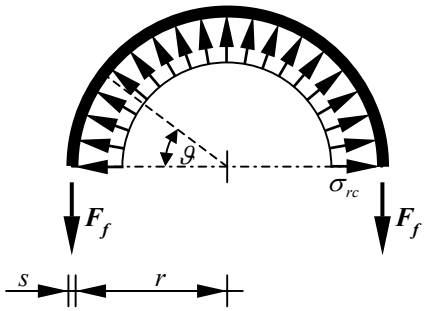

Fig. 30 Static scheme of a unit height FRP strip on the concrete cylinder surface.

For the equilibrium of the unit height strip, it follows that:

$$2s\sigma_f = 2r\int_0^{\pi/2}\sigma_{rc}\,\mathrm{sen}\,\vartheta d\vartheta\,. \qquad (16)$$

In Eq. 16, σ_f represents the stress acting on the unit height strip of thickness *s*:

$$\sigma_f = \frac{F_f}{s}. \qquad (17)$$

From Eq. 16, it follows immediately that:

$$\sigma_{rc} = \frac{s}{r}\sigma_f\,. \qquad (18)$$

For the generic deformed configuration, the confining pressure σ_{rc} is equal to:

$$\sigma_{rc} = \frac{s}{r'}\sigma_f\,. \qquad (19)$$

By substituting Eq. 15 (for unit height) in Eq. 19, one can make the value of σ_{rc} explicit:

$$\sigma_{rc} = \frac{s}{r'}E_f\frac{U-d_{\max}}{r+d_{\max}}\,. \qquad (20)$$

NUMERICAL RESULTS

A preventive numerical analysis has been performed, in such a way as to investigate the sensitivity of the model to the parameter $d_{\max}$. The value of the parameter $d_{\max}$ has been identified by comparison with experimental results, on the base of a parametric analysis.
The comparison between the numeric volume curves for unwrapped and wrapped cylinders is provided in Fig. 31. The qualitative behaviour is in good agreement with the experimental results: -

- The numeric volume curve for unwrapped specimen shows one compressibility zone and one dilatant zone;
- The numeric volume curves for wrapped specimens show two distinct compressibility zones.

In Fig. 32, the numerical axial stress field for the cracked specimen, both in the unwrapped (Fig. 32.a) and wrapped (Fig. 32.b) case, is shown. The relative displacement of the platens is the same for the two specimens. This displacement involves a radial displacement greater than $d_{\max}$ on every cross-section of the wrapped specimen:

$$U > d_{\max} \quad \forall y\,. \qquad (21)$$

In both cases, the stress field has been drawn for the first crack propagation.

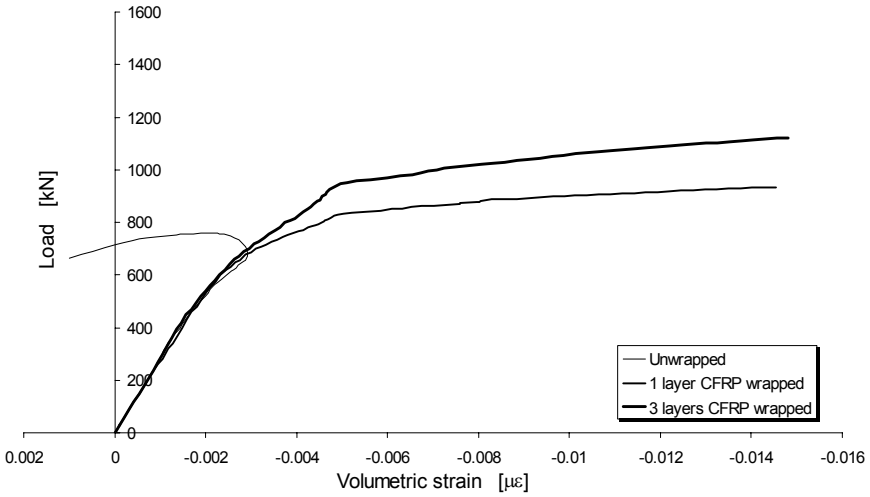

Fig. 31 Numeric volume curves for the unwrapped and the wrapped cylinders.

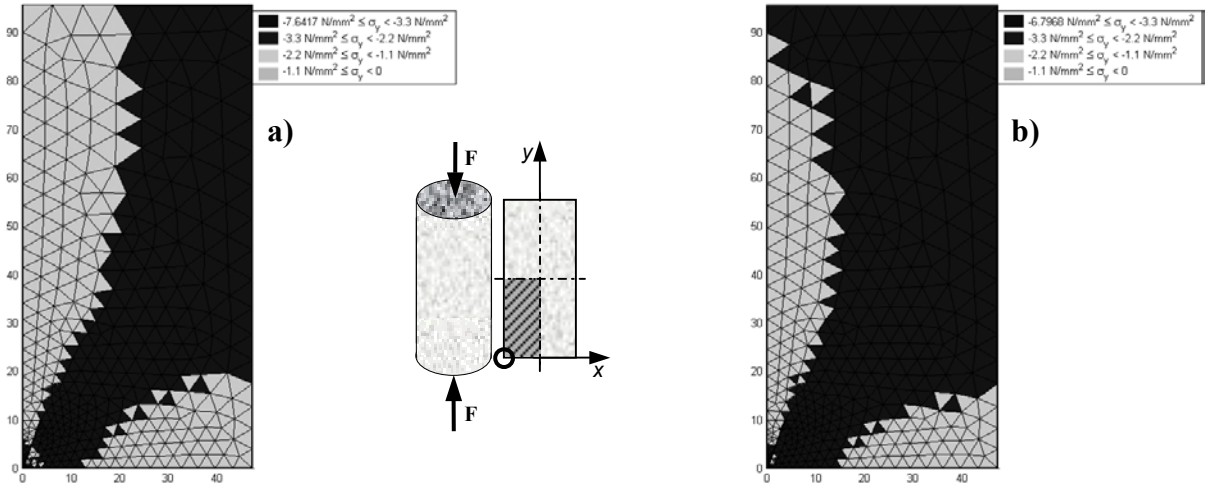

Fig. 32 Axial stress analysis for unwrapped (a) and wrapped (b) specimen.

It can be appreciated how the numerical model is able to take into account stress redistributions for crack propagation, even when the crack path is very short.

The numerical crack path for an advanced stage of crack propagation is shown in Fig. 33.

The mesh generator used in this study is adaptive, and makes it possible to set the mesh size in correspondence of each node. It was chosen to refine the mesh on the crack faces as the crack propagates. The mesh refinement together with the intra-element propagation technique allows the crack path to be accurately predicted[4].

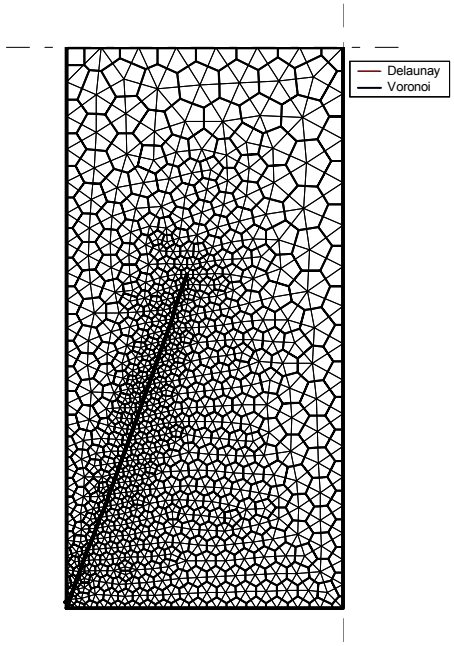

Fig. 33 Numerically predicted crack path for compressive test on concrete cylinders.

With regard to Fig. 32.a, it can also be seen how stress redistribution gives an immediate evaluation of the resistant area decrement with crack propagation. The axial stress on the longitudinal section is actually highly non-homogeneous when crack propagation is activated. A specimen portion unloads for crack propagation, leading to large reductions of effective cross-sectional area. This result validates the base assumption of the Ferretti[2] identifying procedure for concrete effective law. The progressive reduction of effective cross-sectional area, only assumed as a hypothesis by Hudson et al.[43], can now be supported by a numerical analysis.

The wrapping effect on the resistant area decrement can be directly evaluated from stress analysis. Comparison between Fig. 32.a and Fig. 32.b clearly shows how wrapping opposes specimen unloading. Crack paths being equal in both figures, crack edges are partially prevented to open if a wrapping act (Fig. 32.b). Forces can be exchanged on the closed crack edges, as if the crack did not indeed propagate. This leads to an increased resistant area and an increased load carried by the specimen. The assumption of homogeneous state of stress becomes more and more realistic as the number of wrapping sheets is increased. Consequently, the effective behaviour of concrete assumes a greater weight on the overall behaviour of the wrapped specimen as the number of wrapping sheets is increased, while the structural contribution becomes more and more irrelevant. This analysis leads to a new interpretation of experimental data on wrapped specimens. It can actually be stated that the softening disappearance in wrapped specimens should not be associated with the high Young's modulus of the wrapping. It has to be associated with a resistant area close to the nominal area, reducing the gap between material (plain concrete) and specimen behaviour. For a number of FRP sheets sufficient to make the difference between nominal and resistant area negligible, the specimen behaviour turns out to be monotonic non-decreasing, as the effective law is.

In Fig. 34, the numerical load–displacement curves for unwrapped, one layer CFRP wrapped, and three layers CFRP wrapped specimens are shown.

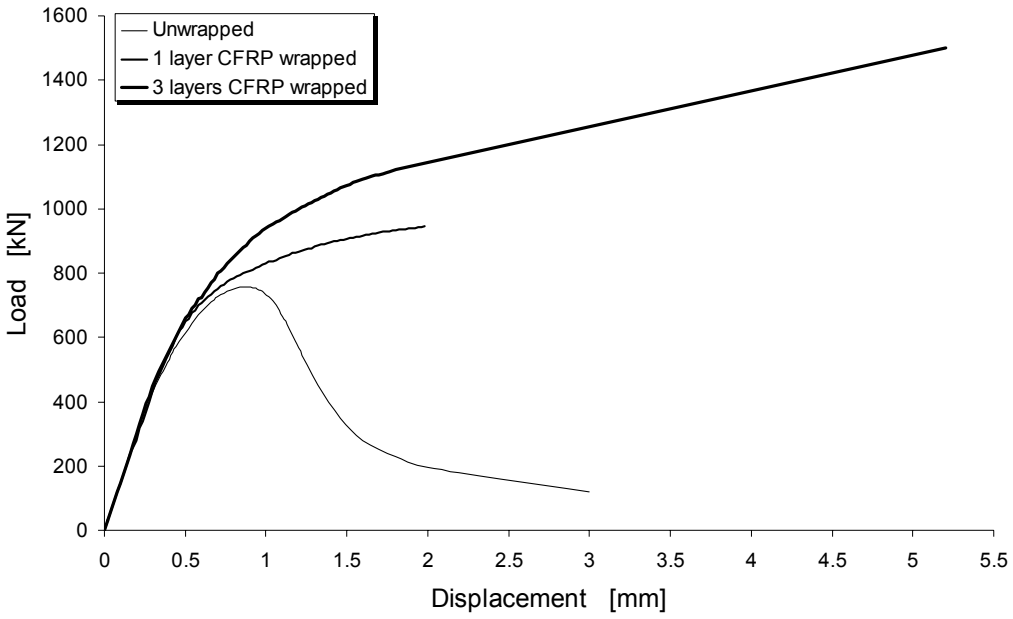

Fig. 34 Numerical load–displacement curves for unwrapped and CFRP wrapped specimens.

The qualitative numerical behaviour is in good agreement with the experimental data: -

- The load–displacement curve for the unwrapped specimen is softening;
- The load–displacement curves for the wrapped specimens are monotonic non-decreasing.

The comparison between numerical and experimental results for each type of considered lateral constraint is provided in Figs. 35÷37.

A similar numerical approach and similar load–displacement results for wrapped cylinders can be found in Harmon et al.[8]. They assumed an elastic linear model for concrete and the shear slip mechanism to cause all non-linear behaviour. Nevertheless, the constitutive choice for concrete is not justified on the base of identifying procedures. It is only a simplified model for numerical simulation. Moreover, crack propagation is not followed step-wise from its initiation forth, which happens for very low values of load. The complete fracture planes are considered to form instantaneously for a load corresponding to the unconfined concrete crush. Starting form this moment, a rough crack model is used to take into account crack slip and separation. This formulation does not allow the model to predict the softening load–displacement curves for unconfined cylinders.

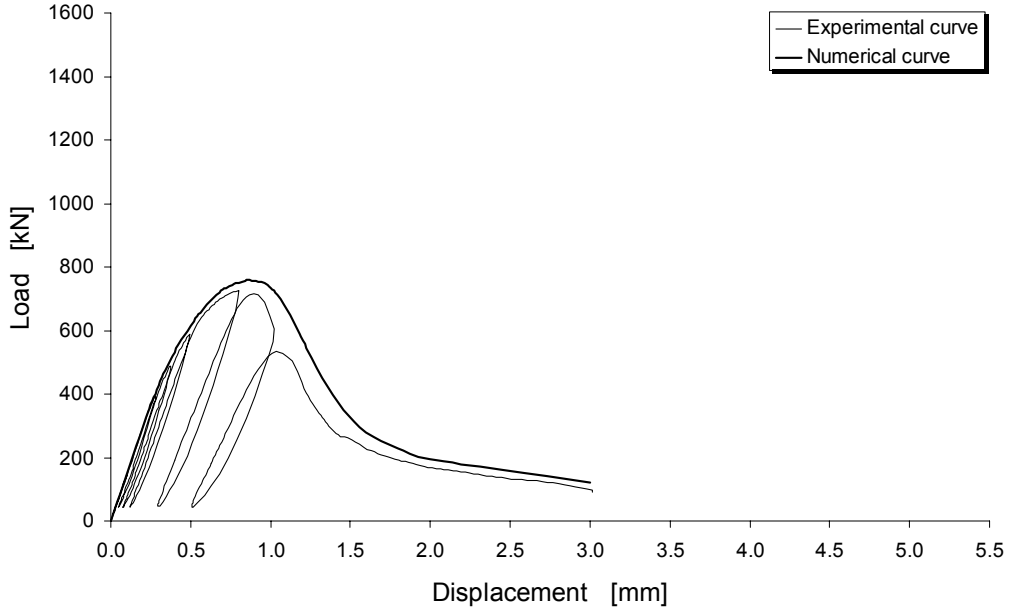

Fig. 35 Comparison between numerical and experimental results for the unwrapped specimen.

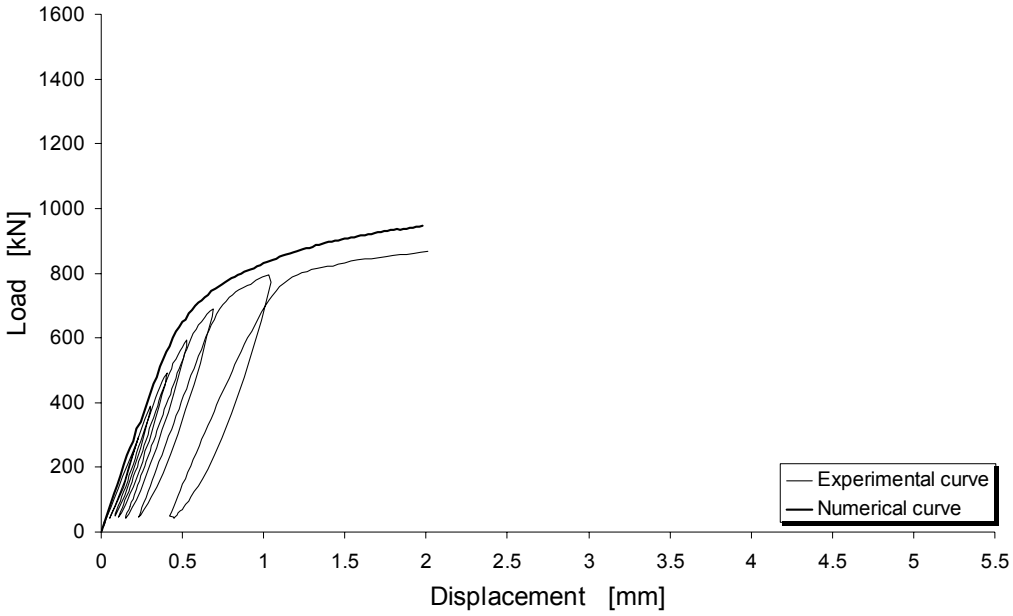

Fig. 36 Comparison between numerical and experimental results for the one layer CFRP wrapped specimen.

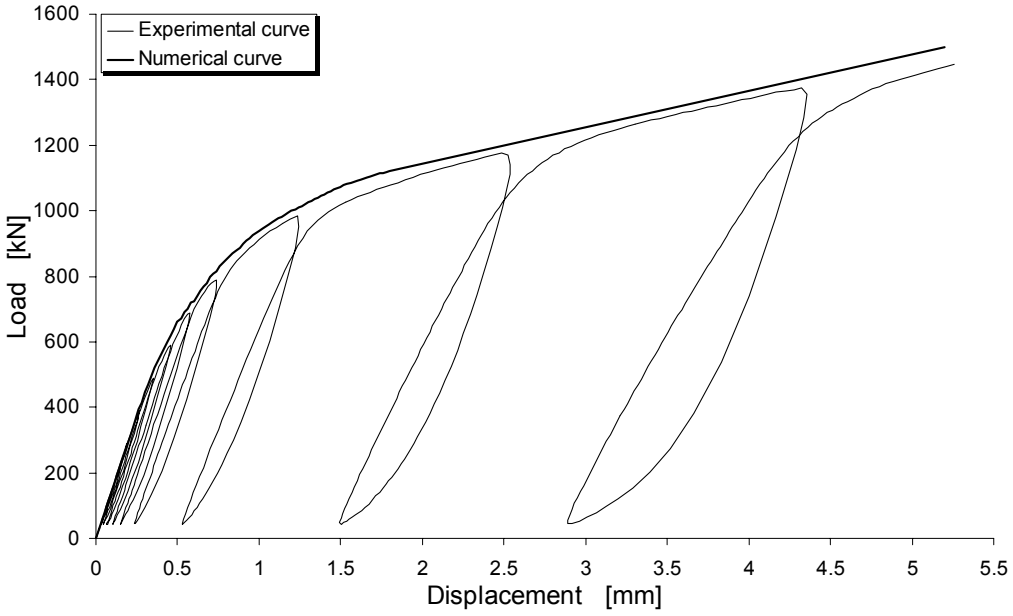

Fig. 37 Comparison between numerical and experimental results for the three layers CFRP wrapped specimen.

CONCLUSIONS

A new constitutive law has been used for analysis of FRP wrapped concrete cylinders. In the aim to separate structural and material behaviour, this law has not been modelled on wrapping tests, but identified on plain concrete tests. It is a simple extension of the effective monoaxial behaviour[2]. No confining effect has been considered.

A numerical code has been presented, allowing accurate dominant crack path predictions in concrete cylinders. The code also makes it possible to estimate stress redistribution and resistant area decrement for crack propagation.

Stiffness decreasing is numerically evaluated as the crack propagates. Influence of the concrete-wrapping interaction on the stiffness is analysed by simply setting the number of wrapping sheets (from 0 to ∞).

The monotone law together with the description of crack propagation are able to reproduce both the softening behaviour of unwrapped specimens and

the monotone behaviour of wrapped specimens. Wrapped cylinders can then be modelled without using modified concrete laws taking into account the triaxial state of stress, as usually done. From the physical viewpoint, this is a notable result. It can actually be stated that models depending on the amount of wrapping are not strictly speaking constitutive. They are models of structural and not material behaviour. Consequently, they are function of a number of parameter to be calibrated on the single test. Here, unwrapped and wrapped behaviour are described by using a single concrete law, only dealing with plain concrete properties. No parameter is needed. This reflects more closely the constitutive nature of the law we are treating with.

The accuracy of the results gives further validation to the Ferretti[2] identification procedure for monoaxial concrete law, which turned out to be monotone. Softening behaviour in unwrapped specimens is no more considered as constitutive. It is imputed to large modifications of in load resistant structure. Monotone behaviour in wrapped specimens is no longer considered as wrapping induced. It is imputed to the wrapping ability to oppose resistant structure modifications. A resistant area closer to the nominal area follows in a specimen behaviour closer to the concrete behaviour, then, monotone.

ACKNOWLEDGEMENTS

This work was made possible by the Italian Ministry for Universities and Scientific and Technological Research (MURST).

All the results here presented are part of the CIMEST Scientific Research on Identification of Materials and Structures – DISTART – Faculty of Engineering – Bologna Alma Mater.

REFERENCES

[1] Ferretti E., Viola E., Di Leo A. and Pascale G., XIV AIMETA, Propagazione della Frattura e Comportamento Macroscopico in Compressione del Calcestruzzo, full test on CD (1999).

[2] Ferretti E., Modellazione del Comportamento del Cilindro Fasciato in Compressione, Ph.D. Thesis, University of Lecce, Italy (2001).

[3] Ferretti E. and Bastianini F., ABDM Symposium, Identification of the Local $\sigma_{eff} - \varepsilon_{eff}$ Law for Concrete Cylinders under Uniaxial Monotone Compression, full test on CD (2002).

[4] Ferretti E., Computer Modeling in Engineering & Sciences, Vol. 4 (2003).

[5] Hanna S. and Jones R., Composite Structures, Vol. 38 (1997), pp. 57-64.

[6] Ghinelli F., Sperimentazione e Modellazione del Comportamento a Compressione del Conglomerato Cementizio Confinato con FRP, Graduation Thesis, University of Bologna, Italy (1997).

[7] Di Leo A., Di Tommaso A. and Merlari R., Technical Note 46, DISTART – University of Bologna, Italy (1979).

[8] Harmon T., Slattery K. and Ramakrishnan S., Non-metallic (FRP) Reinforcement for Concrete Structures, London, U.K. (1995).

[9] Kotsovos M.D. and Pavlović M.N., Ultimate limit-state design of concrete structures – A new approach, London, UK (1999).

[10] Chen W.F. and Ting E.C., Journal of the Engineering Mechanics Division, Vol. 106 (1980), pp. 1-19.

[11] Ahmad S.H. and Shah S.P., Journal of the Structural Division, Vol. 108 (1982), pp. 728-742.

[12] Willam K.J. and Waranke E.P., International Association for Bridge and Structural Engineering, Vol. 19 (1975), pp. 1-30.

[13] Barzegar F. and Maddipudi S., Journal of Structural Engineering, Vol. 123 (1997), pp. 1339-1346.

[14] Mander J.B., Priestley M.J.N., Park R., Journal of Structural Engineering, Vol. 114 (1988), pp. 1827-1849.

[15] Sheikh S.A., ACI Journal, Proceedings (1982), pp. 296-305.

[16] Hoshikuma J., Kawashima K., Nagaya K. and Taylor A.W., Journal of Structural Engineering, Vol. 123 (1997), pp. 624-633.

[17] Kent D.C. and Park R., Journal of the Structural Division, Vol. 97 (1971), pp. 1969-1990.

[18] Muguruma H., Watanabe S., Katsuta S. and Tanaka S., JCA Cement and Concrete, Vol. 34 (1980), pp. 429-432.

[19] Sheikh S.A. and Uzumeri S.M., Journal of Structural Engineering, Vol. 106 (1980), pp. 1079-1102.

[20] Sheikh S.A. and Uzumeri S.M., Journal of Structural Engineering, Vol. 108 (1982), pp. 2703-2722.

[21] Park R., Priestley M.J.N. and Gill W.D., Journal of the Structural Division, Vol. 108 (1982), pp. 929-950.

[22] Fujii M., Kobayashi K., Miyagawa T., Inoue S. and Matsumoto T., JCA Cement and Concrete, Vol. 42 (1988), pp. 311-314.

[23] Mander J.B., Priestley M.J.N., Park R., Journal of Structural Engineering, Vol. 114 (1988), pp. 1804-1826.

[24] Razvi S.R. and Saatcioglu M., ACI Structural Journal, Vol. 86 (1989), pp. 615-623.

[25] Saatcioglu M. and Razvi S.R., Journal of Structural Engineering, Vol. 118 (1992), pp. 1590-1607.

[26] Xie J., Elwi A.E. and MacGregor J.G., Report No. 204, University of Alberta, Edmonton, Alberta, Canada (1994).
[27] Barzegar F. and Maddipudi S., Journal of Structural Engineering, Vol. 123 (1997), pp. 1347-1355.
[28] Richart F.E. et al., Bulletin 185, University of Illinois, Urbana, Illinois (1928).
[29] Miyauchi K., Nishibayashi S., Inoue S., Third International Symposium "Non metallic FRP reinforcement for concrete structures", Estimation of strengthening effects with carbon fiber sheet for concrete column (1997).
[30] Bažant Z.P., Belytschko T.B. and Chang T., Journal of Engineering Mechanics, Vol. 110(1984), pp. 1666-1692.
[31] Hadamard J., Leçons sur la Propagation des Ondes – Chapter VI, Paris, France (1903).
[32] Bažant Z.P. and Belytschko T.B., Journal of Engineering Mechanics, Vol. 111(1985), pp. 381-389.
[33] Bergan P.G., IUTAM W. Prager Symposium, Record of the Discussions on Numerical Modeling (1983).
[34] Hegemier G.A. and Read H.E., DARPA-NSF Workshop, Some Comments on Strain-Softening (1983).
[35] Sandler I. and Wright J.P., DARPA-NSF Workshop, Summary of Strain-Softening (1983).
[36] Wu F.H. and Freud L.B., Report MRL-E-145, Brown University, Providence, RI, USA (1983).
[37] Bažant Z.P., Journal of Engineering Mechanics, Vol. 102 (1976).
[38] Kirkpatrick W.M and Belshaw D.J., Geotechnique, Vol. 18 (1968), pp. 336-350.
[39] Deman F., Dissertation, University of Karlsruhe, Achsensymetrische Spannungs-und Verformungsfelder in trockenem Sand (1975).
[40] Bishop A.W. and Green G.E., Geotechnique, Vol. 15 (1965), pp. 243-266.
[41] Hettler A., Dissertation, University of Karlsruhe, Verschiebungen starrer und elastischer Grundungskörper in Sand bei monotonen und zyklischer Belastung (1981).
[42] Dresher A. and Vardoulakis I., Geotechnique, Vol. 32 (1982), pp. 291-303.
[43] Hudson J.A., Brown E.T. and Fairhurst C., 13th Symposium on Rock Mechanics, Shape of the Complete Stress-Strain Curve for Rock (1971).
[44] Daponte P. and Olivito R.S., ISMM International Conference Microcomputers Applications, Crack Detection Measurements in Concrete, pp.123-127 (1989).
[45] Har J., A New Scalable Parallel Finite Element Approach for Contact-Impact Problems, Ph.D. Thesis, Georgia Institute of Technology, Atlanta (1998).
[46] Papadopoulos P., Jones R.E. and Solberg J., International Journal for Numerical Methods in Engineering, Vol. 38 (1995), pp. 2603-2617.
[47] Zhong Z.H., Finite Element Procedures for Contact-Impact Problems, Oxford/New York/Tokyo (1993), Book review: Applied Mechanics Reviews, Vol. 48 (1995), (written by M Okrouhlik).